A simplified approach to simulate in-plane lateral response of reinforced concrete frames with masonry infills

Mohmad Aslam Sheikh[a], Manish Kumar[a,1] and Rajdeep Ghosh[b]

[a] *Civil Engineering Department, Indian Institute of Technology Gandhinagar, Gandhinagar, India, 382055*

[b] *Deputy Engineer Bridges, Jacobs Solutions India Private Limited, India; formerly, graduate student at Indian Institute of Technology Gandhinagar, India*

ABSTRACT

For seismic design or performance assessment, reinforced concrete (RC) frame buildings with masonry infills are often modeled using strut-cum-masonry constitutive models. A number of models have been considered in the past, which lead to substantially different simulation results. Through an analysis of 106 one-bay-one-story infilled RC frames experimentally studied in the past, this paper presents an evaluation of eight previously proposed masonry constitutive models with masonry panel represented using a set of three struts. The exercise enabled identification of suitable functional forms to characterize the constitutive behavior of masonry panel. Accordingly, a new constitutive model was developed with strength parameters defined in terms of the product of masonry prism strength and cross-sectional area of struts, and stiffness parameters defined in terms of the masonry elastic modulus and cross-sectional area of struts divided by masonry diagonal length. Multipliers were established for ranges of masonry prism strength. In comparison with existing models, the proposed model could effectively capture the response of the 106 specimens despite its simplicity. Simulation results were not significantly correlated with relevant strength parameters of the RC frame, relative stiffness parameter, and observed failure modes. The proposed model can also be used in combination with one or two

[1] Corresponding author.
E-mail address: mkumar@iitgn.ac.in (M. Kumar).

struts. However, one-strut model should be avoided if capturing shear failure in frame members is important.

Keywords: *RC frames; Masonry infill; Shear failure; Flexural failure; Strut models; Masonry constitutive models.*

1. Introduction

Reinforced concrete (RC) frames with unreinforced masonry infill are commonly seen in residential and commercial buildings across the world, and serve as lateral force resisting systems by design or by chance. A number of these buildings have performed reasonably during earthquakes. However, the frame members are vulnerable to flexural and shear failures, and the masonry infill walls often undergo in-plane and out-of-plane failures (especially in the upper stories) [1]-[9]. The in-plane lateral force-displacement response of the infilled RC frames is complex due to the brittle behaviour of masonry panel, and the frame-infill interactions (e.g., [10], [11]). Complexities are further enhanced when a panel has special features (e.g., openings), or when the in-plane and out-of-plane responses are linked (e.g., [12]-[19]).

Infilled RC frames have been modeled using detailed finite element approaches (e.g., [20]-[23]). Such an approach potentially allows capturing global as well local responses of the frame. However, the associated computational costs for realistic building structures can be prohibitive. Besides, the calculated responses may be sensitive to input parameter choices. Therefore, in practical designs and research studies involving realistic or a large number of structural systems, simplistic macro-modeling approach is often adopted (e.g., [24]-[27]). This paper focuses on calculating in-plane response of infilled RC frames through the simplistic models, wherein frame members are considered using line elements capable of capturing flexural, shear and axial responses of the members, and the masonry panel is considered using one or more struts.

Relatively well accepted approaches exist to model the line elements representing the frame members. However, a number of modelling approaches for masonry panel have been used in the past, and a consensus remains elusive. A macro model for masonry panel can be characterized in terms of number and orientation of struts, and associated constitutive properties. Most macro models consider one, two, three or more struts oriented along or around the diagonals of the masonry panel. A number of constitutive models also have been proposed. These models generally start with a strut model, and the parameters of the assumed constitutive model are adjusted to match the experimentally observed response of one-bay-one-story [28]-[29], multi-bay-one-story [28], one-bay-multi-story [10] or multi-bay-multi-story [30]-[31] infilled RC frames. A constitutive model based on the masonry prism tests also has been proposed [32]. The key parameters of these constitutive models typically are peak strength, initial stiffness, deformation corresponding to peak strength (or associated stiffness), residual strength etc. The functional forms for these parameters are chosen based on the basic principles of mechanics (e.g., [10], [11], [28], [30], [32], [33]) or statistical analyses (e.g., [29]). The existing constitutive models have one or more of the following limitations: the calibration of the functional form was performed against a small number (e.g., less than 15) of experimental specimens (e.g., [10], [11], [28], [30], [31], [33]), shear failure in frame members was not considered during calibration (e.g., [10], [29], [31]), interaction between axial force and bending moment capacities (P-M interaction) was ignored (e.g., [10], [29], [31]), interaction between frame and infill was ignored (e.g., [32]), and the experimental dataset did not represent the population either because it was small or because frames with a lower infill strength were more likely to be tested experimentally (e.g., [34]). Further, many constitutive models identified herein consider a single strut to represent the masonry panel for calibration. However, it has been reported that a single-strut model may not adequately capture the lateral force-displacement behaviour of an infilled RC frame, particularly in the post-peak region (e.g., [35]-[37]).

Multiple combinations of strut and constitutive models have been used in the past. For example, single-strut model has been used in combination with constitutive models considered by [10] and [29], two-strut model has been used by [27] and [38], and three-strut model has been used by [39] and [40]. Some studies have been devoted to understand the choice of strut and/or constitutive models on the calculated response of infilled RC frames (e.g., [35], [36], [41]). However, these studies are limited by number of combinations considered (e.g., less than 10), number of experimental specimens (e.g., less than 15), and the parameters of response considered (often limited to initial stiffness, peak strength, and/or visual comparison of the force-displacement response). Expectedly, these evaluations led to divergent conclusions. For example, Asteris et al. [35] found single-strut models inadequate and recommended that a multi-strut model should be used, while Noh et al. [41] based their evaluation on single-strut models. On the other hand, Mohyeddin et al. [36] noted that strut models should be developed specific to frame being studied, which may be impractical, but echoes the observations made by Asteris et al. [35] that macro-modelling of infilled RC frames is an open-ended problem. None of these studies evaluated the performance of the macro-models in capturing the post-peak response of infilled frames, or flexural and shear failures in frame members, which may be important in the collapse assessment of these structures (e.g., [31], [24], [42]).

The choice of strut and constitutive models can impact the conclusions related to calculated performance of a structure. Therefore, it is important to establish some general premises that can guide these choices. Accordingly, the objectives of the present research are: (1) evaluate the performance of constitutive models in simulating the lateral force-displacement response of infilled RC frames, (2) develop a new constitutive model using latest experimental dataset on one-bay-one-story infilled frame with functional forms of the model parameters guided by basic principles of mechanics and results of the first objective, (3) validate the proposed constitutive model, and (4) evaluate the efficacy of single- and two-strut models in combination with the

proposed constitutive model. Cyclic degradation parameters are beyond the scope of present study, as their role is limited in realistic single-event earthquake scenarios (e.g., [43]). A description of the strut and constitutive models is presented in Section 2. Details on 106 one-bay-one-story infilled RC frame specimens experimentally tested in the past are discussed in Section 3. Section 4 presents the modeling approach for infilled RC frames. A numerical model for each of these 106 specimens is developed considering the three-strut and eight constitutive models. Pushover analyses are carried out, and the results are characterized in terms of initial stiffness of the infilled frames, peak strength, secant stiffness corresponding to peak strength, residual strength, post-peak stiffness, and flexural and shear failure in frame members. The approach for characterization is presented in Section 5, and select results are presented in Section 6. A new constitutive model is developed based on three-strut model, and its performance in combination with one-, two- and three-strut models is evaluated in Section 6. Limitations of the proposed model are discussed in Section 7, and the summary and conclusions of this study are presented in Section 8.

2. Macro-models for masonry-infilled RC frames

As noted previously, a macro model for the masonry panel comprises of a strut model and a constitutive model. In the present research, single-strut, two-strut and three-strut models are considered along with eight commonly used constitutive models. The strut and constitutive models are denoted using capital letters S and C, respectively, followed by a serial number. Recognizing that individual strut models have been used with multiple constitutive models in the past, all constitutive models are assumed applicable for all strut models in the present study. A brief description of the three strut and eight constitutive models is provided next.

2.1. Strut models

Fig. 1 shows the three strut models considered in the present study. Solid and broken lines indicate that the strut members are in compression and tension, respectively, when the frame is subjected to a rightward lateral force at the beam level. Equivalent strut width proposed by Mainstone [44], and adopted in design standards and research studies (e.g., [25], [26], [45]), is considered herein:

$$b_m = 0.175(\lambda h)^{-0.4} d_m \tag{1}$$

where b_m is equivalent strut width, h is the height of column, d_m is the diagonal length of masonry panel, and λh is a relative stiffness parameter given by Stafford Smith and Carter [46]

$$\lambda h = h \sqrt[4]{\frac{E_m t_m \sin 2\theta}{4 E_c I_c h_m}} \tag{2}$$

where E_m and E_c are the elastic moduli of masonry and concrete, respectively, I_c is the gross moment of inertia of column cross-section, and t_m and h_m are the thickness and height, respectively, of the masonry wall. Struts are connected to the surrounding frame through a pin.

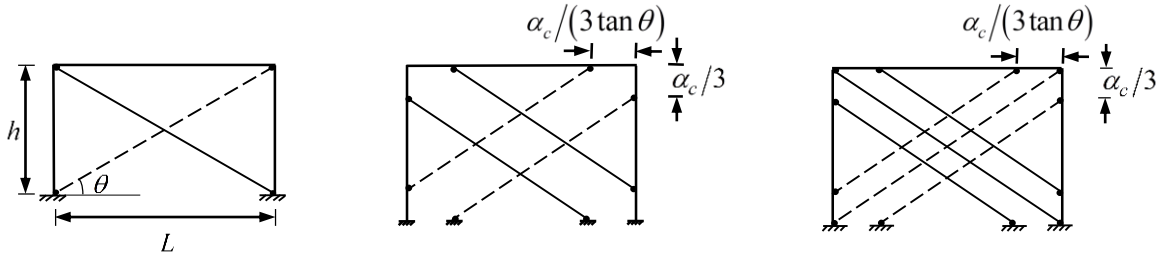

(a) S1 (b) S2 (c) S3

Fig. 1. Strut models (figure partially adapted from Ghosh and Kumar [37]; Reused with permission from The Masonry Society and the 13th North American Masonry Conference)

Strut model S1 (see Fig. 1 (a)) is a commonly used single-strut model (e.g., [10], [29], [47] , [44], [46], [48]). Parameters L and θ in Fig. 1(a) are length of beam and inclination of slope with respect to the horizontal axis, respectively. Strut model S2 (see Fig. 1(b)) has two off-diagonal parallel struts [27]. Each of the two struts account for half of the total strut width

specified in Eq. (1). Model S3 (see Fig. 1(c)) has one diagonal and two parallel off-diagonal struts (e.g., [39]-[40]). The diagonal strut accounts for 50% of the strut width, and the remaining two struts account for 25% each. The contact length α_c given by Stafford Smith and Carter [46] is considered in the present study.

$$\alpha_c = \frac{\pi}{2\lambda} \tag{3}$$

where all parameters were defined previously. The off-diagonal struts in models S2 and S3 are placed at a distance of $\alpha_c/3$ and $\alpha_c/3\tan\theta$ from the beam-column joints along the columns and beam (see Fig. 1), respectively, in line with the approach taken by Smith [49].

2.2. Constitutive material models

Constitutive model C1 is a strut-axial stress-strain relationship proposed by Kaushik et al. [32]. Details of the model (and remaining seven models) are presented in Table 1. The parameters of the model were developed based on five-brick masonry prism tests on 84 specimens with prism strength ranging between 2.9 MPa and 8.5 MPa. Constitutive model C2 was developed by El-Dakhakhni et al. [28]. It was validated against five experimentally tested steel frames with masonry infills. Constitutive model C3 was proposed by Klingner and Bertero [10]. Parameters of the model were calibrated against experimentally observed response of three three-story-one-bay masonry-infilled RC frames with masonry prism strength ranging between 19.0 MPa and 26.4 MPa. Constitutive model C4 is a tetra-linear axial force-displacement relationship for the strut proposed by Panagiotakos and Fardis [30]. Constitutive model C5 is a tri-linear lateral force-displacement relationship developed by Dolsek and Fajfar [47]. Parameters of the model were established based on the tests on 13 specimens [50], wherein masonry prism strength varied between 2 – 5 MPa. Constitutive model C6 was developed by Decanini and Fantin [33], wherein strength corresponding to different failure modes was

considered based on the principles of mechanics and necessary assumptions. Constitutive model C7 is a tri-linear axial force-deformation relationship for the diagonal strut proposed by Burton and Deierlein [31]. Peak strength $\left(F_{\max,e}\right)$ and initial stiffness $\left(K_{1,e}\right)$ for this model was originally given by Paulay and Priestley (1992). The expressions were calibrated against experimental results for 14 infilled RC frames. Constitutive model C8 was developed by Huang et al. [29] based on a dataset of 113 experiments conducted on one-bay-one-story masonry-infilled RC frames. For each experimental specimen, a numerical model was developed wherein the masonry panel was represented using a single strut. The parameters of the backbone and the hysteretic behaviour were established through a calibration exercise.

Table 1. Description of constitutive models

Constitutive model number and reference	Constitutive behavior	Equations	Equation number
C1 Kaushik et al. [32]	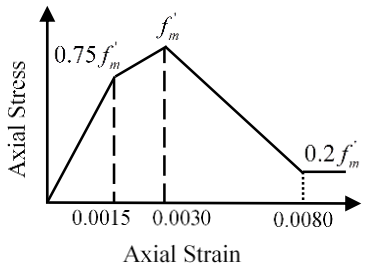	$f_m^{'} = 0.63 f_b^{0.49} f_j^{0.32}$	(4)
C2 El-Dakhakhni et al. [28]	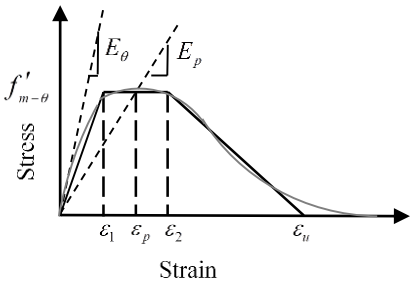	$f_{m-\theta}^{'} = \frac{f_m^{'}}{E} E_\theta$	(5)
		$E_\theta = \frac{1}{\frac{1}{E_0}\cos^4\theta + \left[-\frac{2\nu_{0-90}}{E_0} + \frac{1}{G}\right]\cos^2\theta\sin^2\theta + \frac{1}{E_{90}}\sin^4\theta}$	(6)
		$E_p = 0.5E_\theta$	(7)
		$\varepsilon_p = \frac{f_{m-\theta}^{'}}{E_p}$	(8)
		$\varepsilon_1 = \varepsilon_p - 0.001$	(9)
		$\varepsilon_2 = \varepsilon_p + .0001$	(10)
		$\varepsilon_u = 0.01$	(11)
C3 Klingner and Bertero [10]	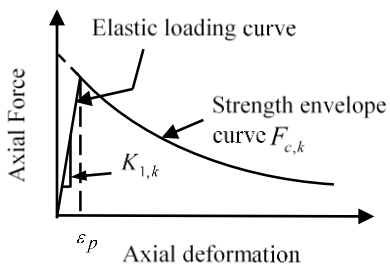	$F_{c,k} = Af_m^{'}(e^{\gamma\nu})$	(12)
		$K_{1,k} = \frac{EA}{d_m}$	(13)

C4
Panagiotakos and Fardis [30]

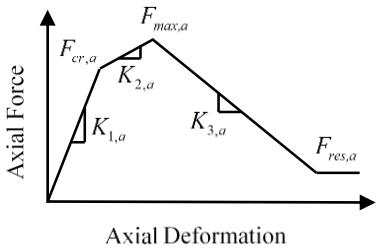

$$F_{cr,a} = f_{tp} t_m l_m \quad (14)$$

$$K_{1,a} = \frac{G t_m l_m}{h_m} \quad (15)$$

$$F_{\max,a} = 1.3 F_{cr,a} \quad (16)$$

$$K_{2,a} = \frac{E_m t_m b_m}{d_m} \quad (17)$$

$$K_{3,a} = 0.005 - 0.100 K_{1,a} \quad (18)$$

$$F_{res,a} = 0.05 - 0.10 F_{max,a} \quad (19)$$

C5
Dolsek and Fajfar [47]

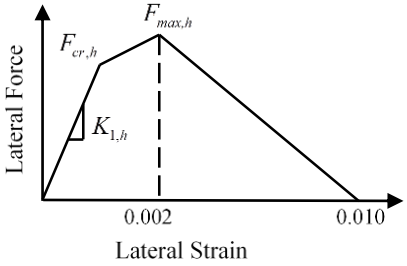

$$F_{cr,h} = 0.6 F_{max,h} \quad (20)$$

$$K_{1,h} = \frac{G t_m l_m}{h_m} \quad (21)$$

$$F_{\max,h} = 0.818 \frac{L_m t_w f_{tp}}{C_I} \left(1 + \sqrt{C_I^2 + 1}\right) \quad (22)$$

C6
Decanini and Fantin [33]

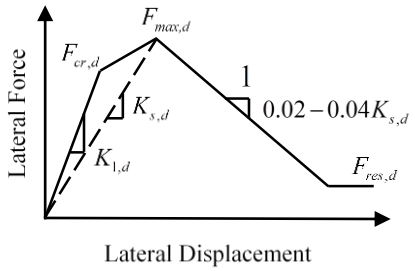

$$F_{cr,d} = 0.8 F_{max,d} \quad (23)$$

$$K_{1,d} = 3K_{t0} + 4K_{s,d} \quad (24)$$

$$F_{\max,d} = \min \begin{cases} \left(0.6 f_{tp} + 0.3\sigma_0\right) t_m d_m \\ \left((1.2\sin\theta + 0.45\cos\theta)\tau_0 + 0.3\sigma_0\right) t_m d_m \\ \dfrac{1.12\sin\theta\cos\theta}{K_{1C6}(\lambda h)^{-0.12} + K_{2C6}(\lambda h)^{0.88}} f'_m t_m b_m \\ \dfrac{1.16\tan\theta}{\lambda h} f'_m t_m b_m \end{cases} \quad (25)$$

$$K_{s,d} = \frac{E_m t_m b_m}{d_m} \quad (26)$$

$$F_{res,d} = 0.35 F_{max,d} \quad (27)$$

C7
Burton and Deierlein [31], Paulay and Priestley [11]

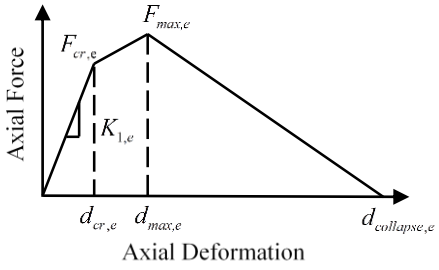

$$F_{cr,e} = \frac{F_{max,e}}{1.3} \quad (28)$$

$$K_{1,e} = \frac{E_m t_m w}{d_m} \quad (29)$$

$$F_{\max,e} = \frac{2}{3} \alpha_c t f'_m \sec\theta \quad (30)$$

$$d_{max,e} = 2 d_{cr,e} \quad (31)$$

$$d_{collapse,e} = 5 d_{max,e} \quad (32)$$

C8
Huang et al. [29]

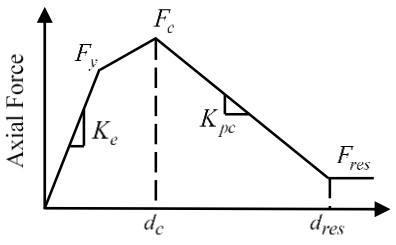

$$F_y = 0.72 F_c \quad (33)$$

$$K_e = 0.0143 E_m^{\,0.618} t_m^{0.694} \left(\frac{h_m}{l_m}\right)^{-1.096} \quad (34)$$

$$F_c = 0.003766 f_m'^{0.196} t_m^{0.867} d_m^{0.792} \quad (35)$$

$$d_c = 0.0154 E^{-0.197} \left(\frac{h_m}{l_m}\right)^{0.978} d_m \quad (36)$$

$$F_{res} = 0.4 F_c \quad (37)$$

$$K_{pc} = -1.278 f_m'^{-0.357} t_m^{\,-0.517} \quad (38)$$

f_b : compressive strength of brick units;

f_j : compressive strength of mortar;

f'_m : masonry prism strength;

τ_0 : sliding resistance in the joints;

A : area of strut;

w : equivalent strut width $\left(= d_m / 4\right)$;

E_0 : elastic modulus parallel to bed joints of masonry wall;	l_m : length of infill wall;
E_{90} : elastic modulus normal to bed joint;	d_m : diagonal length of strut;
ν : axial deformation in the strut;	K_{t0} : elastic stiffness of frame;
γ : strength degradation parameter;	$C_I = 1.925 l_m / h_m$;
f_{tp} : cracking strength obtained from diagonal compression test;	K_{1C6} and K_{2C6} : constants depending on relative stiffness parameter λh ;
σ_0 : vertical stress due to gravity loads;	

The numerical model used to develop models C3, C5, C6 and C8 did not consider P-M interaction in the frame members, which may impact the calculation of nonlinear response of frame and strut representing masonry. Some other constitutive models (e.g., C1) did not consider the frame-infill interaction. Many models (e.g., C3, C5, C8) used a single strut to represent masonry panel that may not adequately capture the distribution of forces along frame members (e.g., [35]-[37]), which may lead to errors in the numerically calculated parameters for masonry panels. Two models (C2 and C3) did not consider the stiffness associated with the stress level corresponding to initial cracking in masonry, which may influence the assessment of the earthquake loads on a structure. Constitutive model C8 was based on the most extensive experimental dataset among all constitutive models considered here. Of the 113 specimens considered to develop the model, 64%, 19%, 10%, 5% and 3% specimens had masonry prism strength ranging between 0 – 5 MPa, 5 – 10 MPa, 10 – 15 MPa, 15 – 20 MPa and 20 – 32 MPa, respectively. It should be noted that masonry prism strength significantly influences the response of infilled RC frames (e.g., [43]). This distribution of masonry prism strength in the dataset can be attributed to a greater likelihood of a specimen with a lesser masonry prism strength being tested in the laboratory, implying that the sample may not be representative of the population due to a systematic bias. While some statistical corrections are possible in the case of "missing information" (e.g., [51]), the extent of the missing data and sensitivity of the regression coefficients towards the same need to be investigated. This problem can partly be addressed by considering ranges of masonry prism strength. The constitutive models discussed in this section use different functional forms to characterize model parameters (e.g., peak strength). Most appropriate functional forms need to be established. A model based on a simple and intuitive

functional forms is more likely to be used in further research and structural design, which motivates the present study.

3. Experimental specimens

Huang et al. [29] considered an extensive experimental dataset on one-bay-one-story infilled RC frames for the development of constitutive model C8. Of the 113 specimens considered by Huang et al. [29], seven studied by Angel et al. [52] were dropped for the present study as the specimens were tested for small deformations only, two studied by Chiou and Hwang [53]) were dropped because these were not strictly one-bay-one-story frames, and four studied by [54], [55], [56] were dropped because the information on some geometrical or material properties was missing. Besides, six specimens studied by [57], [58], [59] not considered by Huang et al. [29] were included in the database, making it a total of 106 specimens considered in the present study. The geometric and material properties of the specimens, and key features of the experiments are presented in Table 2. Scale of specimens ranged between 0.2 and 1, aspect ratio h/L ranged between 0.41 and 1.36, compressive strength of concrete ranged between 9.7 MPa and 65.9 MPa, and compressive strength of masonry prisms ranged between 0.8 MPa and 26.7 MPa. One hundred and four specimens were tested under cyclic loading, while two were tested monotonically. Vertical loads were applied on columns in 85 of 106 specimens. The experimentally recorded force-displacement curves were digitized manually. It should be noted that the present study considers the curve joining the points corresponding to local maxima and minima in line with prior studies (e.g., [41], [60], [61]). The experimental backbone considered in the present study is the average of those in the positive and negative displacement directions, in case the loading was cyclic.

Table 2. List of experimental specimens

Reference	Scale	Tag	$h \times L$ (m × m)	Aspect ratio	Cross section (mm × mm)		Compressive strength (MPa)		Elastic Modulus[3] (MPa)	Load[1]	Vertical load[2]
					Column	Beam	Concrete $\left(f_c^{'}\right)$	Masonry $\left(f_m^{'}\right)$	Masonry $\left(E_m\right)$		
Mehrabi et al. **[60]**	1/2	E1	1.54 × 2.31	0.66	178 × 178	152 × 229	26.8	10.6	4595.63	C	Yes
		E2	1.54 × 2.31	0.66	178 × 178	152 × 229	20.9	13.9	8943.22	C	Yes
		E3	1.54 × 2.34	0.66	203 × 203	152 × 229	25.8	10.1	4196.01	C	Yes
		E4	1.54 × 2.34	0.66	203 × 203	152 × 229	33.4	13.6	9067.24	C	Yes
		E5	1.54 × 3.12	0.49	178 × 178	152 × 229	26.9	10.6	3941.08	C	Yes
		E6	1.54 × 3.12	0.49	178 × 178	152 × 229	25.7	11.4	9597.77	C	Yes
Basha and Kaushik **[61]**	1/2	E7	1.59 × 1.68	0.95	115 × 175	115 × 175	22.4	3.9	2700.00	C	Yes
		E8	1.59 × 1.68	0.95	115 × 175	115 × 175	22.4	3.9	2700.00	C	Yes
		E9	1.59 × 1.68	0.95	115 × 175	115 × 175	22.4	4.6	2800.00	C	Yes
		E10	1.59 × 1.68	0.95	115 × 175	115 × 175	22.4	4.6	2800.00	C	Yes
Al-Chaar et al. [57]	1/2	E11	1.43 × 2.03	0.70	127 × 203	127 × 197	38.4	18.2	-	M	No
		E12	1.43 × 2.03	0.70	127 × 203	127 × 197	38.4	26.7	-	M	No
Kakaletsis and Karayannis [62]	1/3	E13	0.9 × 1.35	0.67	150 × 150	100 × 200	28.5	2.6	660.66	C	Yes
		E14	0.9 × 1.35	0.67	150 × 150	100 × 200	28.5	15.2	2837.14	C	Yes
Colangelo [50]	1/2	E15	1.43 × 1.90	0.75	200 × 200	200 × 250	43.7	5.1	4230.00	C	Yes
		E16	1.43 × 1.90	0.75	200 × 200	200 × 250	46.5	5.1	4230.00	C	Yes
		E17	1.43 × 2.50	0.57	200 × 200	200 × 250	51.2	5.1	4230.00	C	Yes
		E18	1.43 × 2.50	0.57	200 × 200	200 × 250	48.9	5.1	4230.00	C	Yes
		E19	1.43 × 2.50	0.57	200 × 200	200 × 250	44.5	2.7	1212.00	C	Yes
		E20	1.43 × 2.50	0.57	200 × 200	200 × 250	54.6	2.7	1212.00	C	Yes
		E21	1.43 × 1.90	0.75	200 × 200	200 × 250	35.6	2.2	-	C	Yes
		E22	1.43 × 1.90	0.75	200 × 200	200 × 250	41.3	2.2	-	C	Yes
		E23	1.43 × 2.50	0.57	200 × 200	200 × 250	39.6	2.2	-	C	Yes
		E24	1.43 × 2.50	0.57	200 × 200	200 × 250	42.5	2.2	-	C	Yes
		E25	1.43 × 2.50	0.57	200 × 200	200 × 250	41.7	2.2	-	C	Yes
Combescure and Pegon [63]	1/2	E26	1.72 × 2.30	0.75	150 × 150	150 × 200	20.0	2.2	-	C	Yes
Cai and Su [59]	1	E27	3.23 × 4.40	0.73	400 × 400	200 × 450	33.5	4.2	-	C	Yes
		E28	3.23 × 4.40	0.73	400 × 400	200 × 450	33.5	2.0	-	C	Yes
Blackard et al. [64]	2/3	E29	2.05 × 3.66	0.56	279 × 279	279 × 368	19.1	19.1	-	C	Yes
Alwashali et al. [58]	1/2	E30	1.60 × 2.30	0.70	200 × 200	600 × 400	24.2	17.3	-	C	Yes
		E31	1.60 × 2.30	0.70	300 × 300	600 × 400	28.3	18.6	-	C	Yes
Dautaj et al. [65]	2/3	E32	2.10 × 2.65	0.79	150 × 150	150 × 200	24.5	3.99	2192.99	C	Yes
		E33	2.10 × 2.65	0.79	150 × 150	150 × 200	24.5	2.03	1121.23	C	Yes
		E34	2.10 × 2.60	0.81	150 × 200	150 × 200	24.0	3.99	2192.99	C	Yes
		E35	2.10 × 2.60	0.81	150 × 200	150 × 200	24.5	3.99	2192.99	C	Yes
		E36	2.10 × 2.55	0.82	150 × 250	150 × 250	25.0	3.99	2192.99	C	Yes
		E37	2.10 × 2.65	0.79	150 × 150	150 × 200	24.0	3.69	10058.07	C	Yes
		E38	2.10 × 2.50	0.84	150 × 300	150 × 300	24.5	5.25	2885.51	C	Yes
Gazic and Sigmund [66]	1/2	E39	1.41× 2.0	0.71	125 × 150	125 × 200	20.0	4.6	8182.37	C	Yes
		E40	1.41× 2.0	0.71	125 × 150	125 × 200	20.0	4.6	8182.37	C	Yes
		E41	1.41× 2.0	0.71	125 × 150	125 × 200	20.0	5.2	1663.85	C	Yes
		E42	1.41× 2.0	0.71	125 × 150	125 × 200	20.0	0.8	1764.78	C	Yes
		E43	1.41× 2.0	0.71	125 × 150	125 × 200	20.0	3.5	1651.86	C	Yes
		E44	1.41× 2.0	0.71	125 × 150	125 × 200	20.0	5.2	1663.85	C	Yes
		E45	1.41× 2.0	0.71	125 × 150	125 × 200	20.0	4.6	8182.37	C	Yes
		E46	1.41× 2.0	0.71	125 × 150	125 × 200	20.0	5.2	1663.85	C	Yes
		E47	1.41× 2.0	0.71	125 × 150	125 × 200	20.0	4.6	8182.37	C	Yes
		E48	1.41× 2.0	0.71	125 × 150	125 × 200	20.0	5.2	1663.85	C	Yes
Bergami and Nuti [67]	1/2	E49	1.42× 2.5	0.57	200 × 200	200 × 250	30.0	6.2	1666.52	C	Yes
		E50	1.42× 2.5	0.57	200 × 200	200 × 250	30.0	6.2	1666.52	C	Yes
Mansouri et al. [68]	1/2	E51	1.38× 2.30	0.60	200 × 200	200× 150	21.9	2.30	436.69	C	Yes
Misir et al. [69]	4/5	E52	2.20 × 3.60	0.61	250 × 400	250 × 400	27.1	1.5	840.92	C	Yes
		E53	2.20 × 3.60	0.61	250 × 400	250 × 400	26.4	2.1	1158.09	C	Yes
		E54	2.20 × 3.60	0.61	250 × 400	250 × 400	24.5	2.4	1314.82	C	Yes
		E55	2.20 × 3.60	0.61	250 × 400	250 × 400	26.8	1.6	854.30	C	Yes
		E56	2.20 × 3.60	0.61	250 × 400	250 × 400	25.5	1.8	1005.78	C	Yes
Morandi et al. [70]	1/2	E57	3.12 × 4.55	0.69	350 × 350	350 × 350	34.0	4.6	5295.35	C	No[2]
		E58	3.12 × 4.55	0.69	350 × 350	350 × 350	34.0	4.6	5295.35	C	No[2]
		E59	3.12 × 4.55	0.69	350 × 350	350 × 350	34.0	4.6	5295.35	C	No[2]
Tizapa [71]	1/1	E60	2.10 × 2.70	0.78	125× 200	125× 200	24.0	4.5	2424.33	C	No
Verderame et al. [72]	1/3	E61	1.47 × 2.30	0.64	200 × 200	200 × 250	22.7	3.2	-	C	Yes
		E62	1.47 × 2.30	0.64	200 × 200	200 × 250	21.3	3.2	-	C	Yes

Akhoundi et al. [73]	1/2	E63	1.77 × 2.86	0.62	160 × 160	160 × 270	20.0	2.0	-	C	Yes
Chiou and Hwang [53]	1/1	E64	2.94 × 3.60	0.82	350 × 400	350 × 600	25.0	7.0	-	C	No
		E65	2.94 × 3.60	0.82	350 × 400	350 × 600	27.0	8.5	-	C	No
Zovkic et al. [74]	1/2.5	E66	2.05 × 3.66	0.56	200 × 200	120 × 200	51.5	4.3	-	C	Yes
		E67	2.05 × 3.66	0.56	200 × 200	120 × 200	48.5	1.9	-	C	Yes
		E68	2.05 × 3.66	0.56	200 × 200	120 × 200	35.0	1.6	-	C	Yes
Kumar [75]	1/1	E69	2.41 × 2.50	0.96	150 × 300	150 × 600	30.0	0.9	-	C	No
Bose and Rai [76]	1/2.5	E70	1.23 × 3.00	0.41	200 × 200	200 × 200	37.6	2.4	-	C	Yes
Leuchars and Scrivener [77]	1/1	E71	1.27× 1.96	0.65	203 × 152	203 × 152	24.8	3.8	-	C	No
Schwarz et al. [78]	1/2	E72	1.50× 1.10	1.36	200 × 200	100 × 200	28.8	2.7	-	C	Yes
		E73	1.50× 2.24	0.67	200 × 200	100 × 200	28.8	2.7	-	C	Yes
Zhai et al. [79]	1/1	E74	2.80 × 3.15	0.89	352× 352	350 × 400	27.7	1.9	-	C	Yes
Stylianidis [80]	1/3	E75	0.96 × 1.60	0.60	150 × 150	100 × 200	26.5	4.2	-	C	No
		E76	0.96 × 1.01	0.95	150 × 150	100 × 200	27.9	1.9	-	C	No
Cavaleri et al. [81]		E77	1.80 × 1.80	1.00	200 × 200	200 × 400	25.0	2.7	3930.29	C	Yes
		E78	1.80 × 1.80	1.00	200 × 200	200 × 400	25.0	2.7	3930.29	C	Yes
		E79	1.80 × 1.80	1.00	200 × 200	200 × 400	25.0	8.7	6396.59	C	Yes
		E80	1.80 × 1.80	1.00	200 × 200	200 × 400	25.0	8.7	6396.59	C	Yes
		E81	1.80 × 1.90	0.95	300 × 300	300 × 400	25.0	1.7	4561.86	C	Yes
		E82	1.80 × 1.90	0.95	300 × 300	300 × 400	25.0	1.7	4561.86	C	Yes
		E83	1.80 × 1.90	0.95	300 × 300	300 × 400	25.0	1.7	4561.86	C	Yes
		E84	1.80 × 1.90	0.95	300 × 300	300 × 400	25.0	1.7	4561.86	C	Yes
		E85	1.80 × 1.80	1.00	200 × 200	200 × 400	25.0	4.6	7101.11	C	Yes
		E86	1.80 × 1.80	1.00	200 × 200	200 × 400	25.0	4.6	7101.11	C	Yes
		E87	1.80 × 1.80	1.00	200 × 200	200 × 400	25.0	8.7	6396.59	C	Yes
		E88	1.80 × 1.80	1.00	200 × 200	200 × 400	25.0	8.7	6396.59	C	Yes
Baran and Sevil [82]	1/3	E89	0.82 × 1.40	0.58	150 × 100	150 × 150	15.6	3.2	-	C	Yes
		E90	0.82 × 1.40	0.58	150 × 100	150 × 150	10.7	3.0	-	C	Yes
		E91	0.82 × 1.40	0.58	150 × 100	150 × 150	9.7	3.0	-	C	Yes
Crisafulli [83]	3/4	E92	2.10 × 2.67	0.79	150 × 150	150 × 200	22.5	19.3	11542.05	C	Yes
		E93	2.10 × 2.67	0.79	150 × 150	150 × 200	31.2	19.3	11542.05	C	Yes
Calvi and Bolognini [84]	1/1	E94	2.90 × 4.50	0.64	300 × 300	700 × 250	29.3	1.1	1871.71	C	No[2]
Tawfik and Essa [85]	1/2	E95	1.60× 1.98	0.80	120 × 200	120 × 200	65.0	4.0	2192.99	C	No[2]
		E96	1.60× 1.98	0.80	120 × 200	120 × 200	66.0	3.4	1896.19	C	No[2]
		E97	1.60× 1.98	0.80	120 × 200	120 × 200	66.0	1.9	1071.76	C	No[2]
Basha and Kaushik [61]	1/2	E98	1.59 × 1.68	0.95	115 × 175	115 × 175	22.4	3.9	2698.14	C	Yes
		E99	1.59 × 1.68	0.95	115 × 175	115 × 175	22.4	3.9	2698.14	C	Yes
Haider [86]	1/1	E100	2.20 × 2.26	0.97	254 × 254	254 × 254	34.3	10.8	2344.67	C	No[2]
		E101	2.20 × 2.20	1.00	305 × 305	254 × 254	35.2	12.1	2248.21	C	No[2]
		E102	2.20 × 1.80	1.22	254 × 254	254 × 254	37.5	18.1	3219.70	C	No[2]
		E103	2.20 × 1.80	1.17	305 × 305	305 × 254	38.2	17.4	3203.16	C	No[2]
Sigmund [87]	1/2.5	E104	1.40 × 2.00	0.70	200 × 200	120 × 200	45.0	2.7	3204.16	C	Yes
Yuksel **[88]**	1/2	E105	1.36 × 1.95	0.70	200 × 250	200 × 325	18.0	25.3	7912.55	C	No[2]
Bellington et al. [89]	1/5	E106	0.63 × 1.1	0.57	165 × 108	165 × 140	20.7	20.1	5119.30	C	Yes

[1]M – Monotonic; C – Cyclic

[2]Vertical loads were applied on the beam during experiments, but the magnitude of the load was small.

[3]The elastic modulus of masonry panel was considered as $\left(E_m = 550 \times f_m^{'}\right)$ in case not provided.

4. Modelling masonry-infilled RC frames

Fig. 2 presents a schematic of the model for the infilled RC frames. There are nine frame elements (numbered 1 through 9) in series with nine shear hinge elements, and struts representing the masonry infill panel; solid (broken) lines indicate that the strut will be in compression (tension) when a lateral load to the right is applied at the beam level.

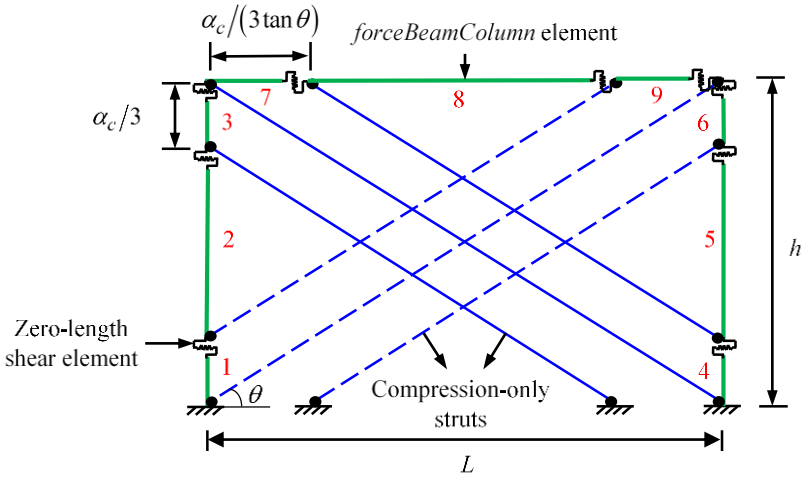

Fig. 2. A schematic of a three-strut model (adapted from Ghosh and Kumar [37]); Figure reused with permission from TMS and 13NAMC)

The open source software program OpenSees [90] is considered for lateral pushover analyses. Beams and columns of a frame are modelled using the distributed plasticity approach, which incorporates the P-M interaction in frame members. Flexural behavior of the frame members is simulated using the *forceBeamColumn* element, which is a force-based nonlinear fiber-based beam-column element. Concrete and longitudinal reinforcements are modelled using *fiber* sections. Uniaxial material *Concrete01* is used to model the core (confined) and cover (unconfined) concrete. Stress-strain relationships for the confined and unconfined concrete are defined using the model proposed by Mander et al. [91]. Reinforcements are modelled using *Steel01*, which is a uniaxial bilinear steel material object with kinematic hardening. Reinforced concrete members may be vulnerable to shear failure before or after flexural failure has taken place. Several models to describe shear force-displacement behavior of RC members have been proposed (e.g., [92]-[94]). In the present study, the model proposed by Elwood [93] has been considered, wherein shear strength is based on Sezen and Moehle [94]. Shear behavior of RC members is modelled using *zeroLength* elements placed in series with frame members. *LimitStateMaterial* material available with OpenSees is used to implement the material model.

Struts representing masonry panels are modelled using *forceBeamColumn* element. These are connected to the frame through a pin, and resist forces only in compression. Uniaxial material

object *Pinching4* is used to define the constitutive model for the struts. Cyclic degradation and pinching parameters used for the *Pinching4* material are based on Kumar et al. [43]. It should be noted that the central goal of this work is to characterize the backbone curves obtained through monotonic analysis. Accordingly, the degradation parameters do not influence the results presented in this study. Secondly, the influence of the choice of degradation parameters on the lateral force-displacement response of an infilled RC frame subjected to a realistic earthquake scenario is considerably less compared to that of the backbone curve [43].

Vertical loads were applied on most specimens. These loads are considered in the analytical models as follows. Loads applied directly on the columns during experiments are applied directly on the columns in the models. Loads applied on the beams during experiments are applied directly on the top of columns considering the beam to be simply supported on the column. It is recognized that a fraction of the load could have gone through the masonry panel, which is not possible to simulate through the analytical models considered herein.

All analyses were displacement-controlled with Gauss-Lobatto integration scheme. *Newton* or *ModifiedNewton* algorithm was used to solve to the equilibrium equations. Command *NormDispIncr* was invoked to establish convergence with a tolerance of 10^{-10} (it was increased up to 10^{-5} in order to achieve convergence at a step).

5. Characterizing performance of macro models

5.1. Backbone parameters

Eight macro models (see Fig. 1(c) and Table 1) were developed for each of the 106 experimental specimens. Monotonic pushover analyses were carried out using each of these models. Simulated results, namely, lateral force-displacement response, and flexural and shear failures in frame members, were compared with corresponding experimental observations. Fig. 3 presents the simulated force-displacement response of experimental specimens DFS of [61]

and WF of [58] using macro model S3-C1 (combination of strut model S3 and constitutive material model C1). Masonry prism strengths for the two specimens are 4 MPa ("weak" infill) and 17.3 MPa ("strong" infill), respectively. Also presented in the figure are the results for macro models S3-C2, S3-C3, S3-C4, S3-C5, S3-C6, S3-C7 and S3-C8, and that observed experimentally. It is clear that the choice of constitutive model significantly influences the lateral force-displacement response of the infilled RC frame. In order to quantify the performance of a macro model (e.g., S3-C6), the calculated lateral force-displacement response is idealized first. Fig. 4 presents a generic lateral force-displacement curve for an infilled RC frame. The response up to the point corresponding to the peak strength can be characterized using the force associated with first major change in stiffness F_1, initial stiffness K_1, and peak force F_2 and associated displacement D_2. These parameters can be compared with that for corresponding experimentally obtained response. The average of the ratios of simulated and experimentally recorded forces at different displacements greater than corresponding experimental value of D_2 can provide information on the ability of a macro model to simulate the post-peak response.

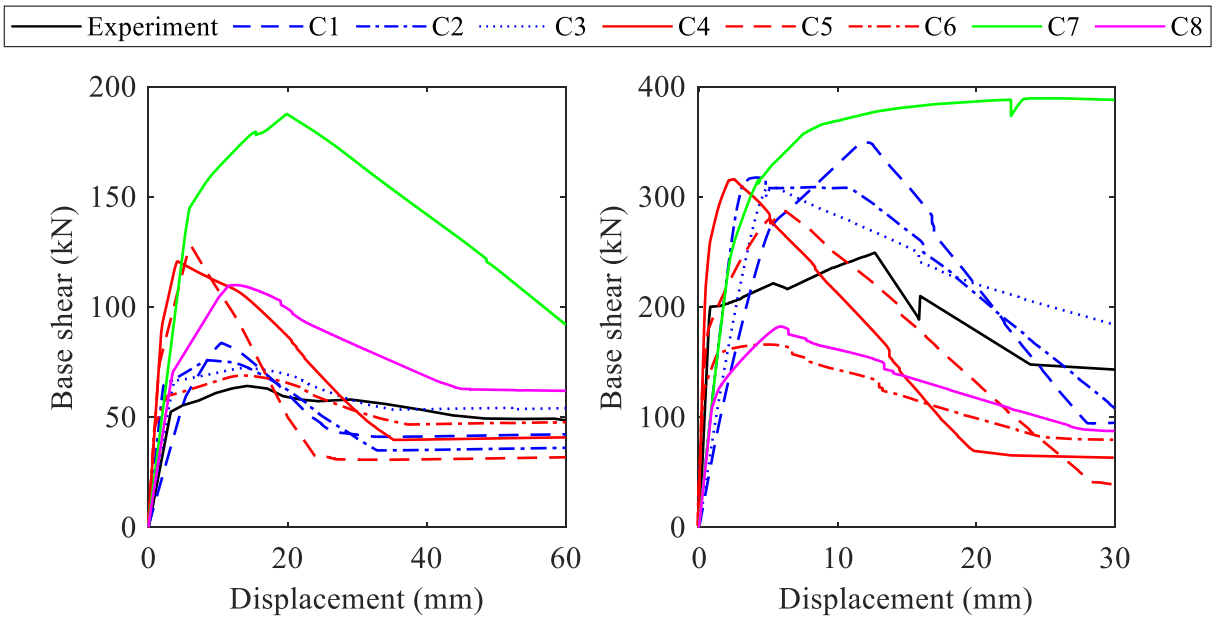

(a) Specimen DFS [61] (b) Specimen WF [58]

Fig. 3. Experimentally observed and simulated force-displacement response for two one-bay-one-story infilled RC specimens.

For an experimentally obtained force-displacement curve, F_2 and D_2 (see Fig. 4) were identified first. The point corresponding to F_1 was identified by judgement. Initial stiffness K_1 was determined as the slope of the first line. The parameters for simulated force-displacement curves were determined through a similar, but automated, approach. Peak force F_2 and corresponding displacement D_2 were identified first. Force F_1 was then determined such that the ratio of the slope of the line between origin and (D_1,F_1), and that between (D_1,F_1) and the point corresponding to $0.85F_2$ was the highest. This approach helped avoid points closer to (D_2,F_2), which may be associated with greater levels of damage.

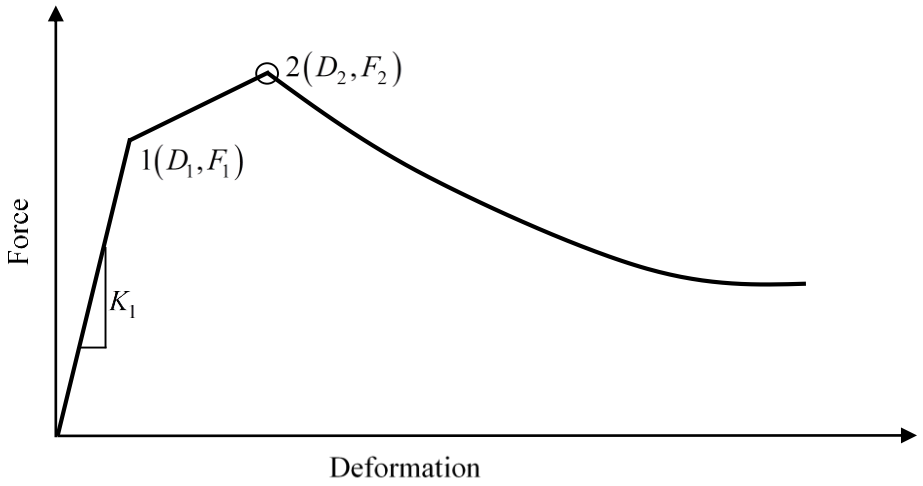

Fig. 4. Idealized backbone curve for masonry-infilled RC frames

Table 3 presents parameters F_1, K_1, F_2 and D_2 corresponding to experimentally recorded force-displacement curve for specimen DFS of [61]. Also included in the table are parameters for the simulated curves obtained using the eight macro models (also see Fig. 3). A total of 10,000 equispaced points were identified between zero displacement and the displacement up to which the experiment was performed. Further, points beyond displacement D_2 (in the post-peak regime) were considered, and simulated and experimental values of forces ordinates were determined. The ratios of simulated values to the corresponding experimental values were calculated for all these points, and their average (R_{PP}) was considered. Parameter R_{PP} is

considered to indicate the strength of simulation in the post-peak region, namely, the simulation using a macro-model is better if the parameter is closer to 1, and vice-versa. Parameter R_{PP} is also reported in Table 3.

Table 3. Simulated and experimental results for DFS specimen of [61] (see Fig. 2 for element numbers)

Experimental specimen	Macro model	K_1	F_1	F_2	D_2	R_{PP}	Elements failed in shear	Elements failed in flexure
		kN/mm	kN	kN	mm			
DFS		16.34	52.15	64.09	14.11	-	Column	Column
	S3-C1	11.02	59.74	83.65	10.51	0.85	-	4,7
	S3-C2	-	-	75.77	8.63	0.78	-	4,7
	S3-C3	-	-	72.22	14.10	1.07	-	4,7
	S3-C4	45.91	92.48	120.67	4.20	0.98	4	4,7
	S3-C5	47.68	72.58	127.69	6.10	0.67	3,4	4,7
	S3-C6	51.77	44.93	68.83	13.65	0.96	-	4,7
	S3-C7	24.52	144.81	187.47	19.90	2.67	3,4,7	4,7
	S3-C8	20.06	70.20	109.87	12.39	1.40	3,4	4,7

5.2. Failure in frame members

Specimen DFS of [61] underwent shear as well as flexural failure during the experiment. Strut model S3 combined with constitutive models C4, C5, C7 and C8 could simulate shear failure in frame members. All combinations of strut (S3) and constitutive (C1 through C8) models could capture flexural failure in frame members. A similar analysis was performed for all 106 experimental specimens. Ratios of simulated values of K_1, F_1, F_2, and D_2 to the respective experimental values were computed (also see [95]). A part of these results is discussed in Section 6, which guides the development of the proposed model.

Information on the flexural and/or shear failures in frame members was reported for 74 experimentally studied specimens [95]. Bending moment developed in a frame member exceeding the corresponding yield strength was considered as flexural failure. Similarly, shear force developed in a frame member exceeding the corresponding strength (e.g., [93]) was treated as shear failure. The ability of a macro model to capture flexure (or shear) failure can be quantified in terms of *correct* and *incorrect* simulations. Say, n_1 is the number of specimens for which a failure was observed during a simulation as well as the corresponding experiment.

Similarly, n_2 is the number of specimens for which failure was not observed in either simulation or experiment. These numbers correspond to *correct* simulations. Say, n_3 (n_4) is the number of specimens for which a failure was experimentally observed but not simulated (experimentally not observed but simulated) using a numerical model. These numbers (n_3 and n_4) correspond to *incorrect* simulations.

6. Proposed macro model

6.1. Development

Strut model S3 is considered for the development of the masonry constitutive model, which is defined using parameters identified in Fig. 5, namely, $F_{cr,\mathrm{m}}$, $K_{1,\mathrm{m}}$, $K_{2,\mathrm{m}}$, $F_{\mathrm{max,m}}$, $K_{3,\mathrm{m}}$, and $F_{res,m}$. These parameters represent first major crack in masonry, initial stiffness, peak strength, secant stiffness corresponding to peak strength, slope for the post-peak segment, and residual strength of the combination of the three struts representing the masonry panel, respectively (also see Table 1). The development of each parameter is discussed in the sections below.

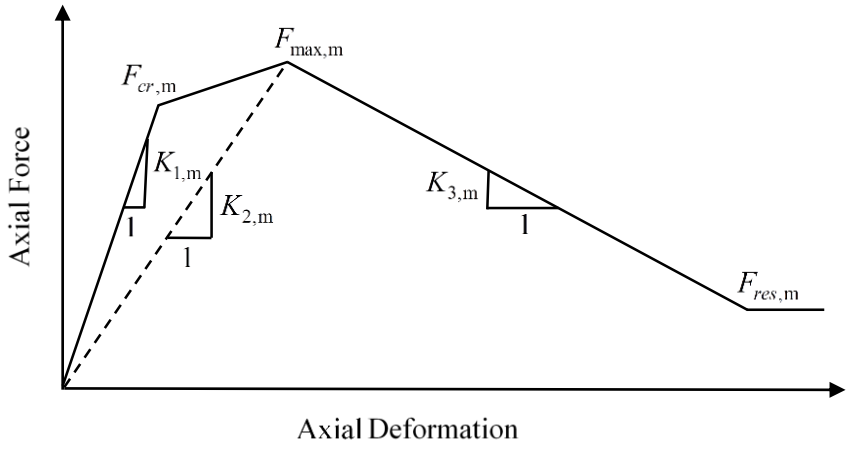

Fig. 5. Backbone curve for the proposed constitutive model

6.1.1. Peak strength $\left(F_{\max,m}\right)$

An attempt was made to characterize the peak strength of masonry prism $F_{\max,m}$ (see Fig. 5) first. For the 106 one-bay-one-story infilled RC frames (see Table 2), Table 4 presents the mean of the simulated-to-experimental (S/E) ratios of peak strength of infilled RC frame F_2 (see Fig. 4). The simulations were performed using eight macro models, namely, S3-C1 through S3-C8 (see Fig. 2 for the schematic, and Table 1 for the details of masonry constitutive models C1 through C8 developed in the prior studies). Table 4 also presents standard deviations (STDs) and coefficients of variation (COVs) associated with the S/E ratios.

Table 4. Mean simulated-to-experimental (S/E) ratios, corresponding standard deviations (STDs) and coefficients of variation (COVs) for peak strength of infilled RC frame

			$0 < f_m^{'} < 5$ MPa			$5 < f_m^{'} < 10$ MPa			$f_m^{'} > 10$ MPa		
Parameter	CM	Eq.	Mean	STD	COV	Mean	STD	COV	Mean	STD	COV
F_2	C1	(4)	**0.93**	**0.36**	**0.38**	**0.99**	**0.25**	**0.25**	**1.61**	**0.79**	**0.49**
	C2	(5)	0.84	0.33	0.39	0.93	0.23	0.25	1.54	0.83	0.54
	C3	(12)	0.82	0.29	0.36	0.89	0.23	0.26	1.46	0.83	0.57
	C4	(16)	1.34	0.55	0.41	1.14	0.26	0.23	1.48	0.85	0.58
	C5	(22)	1.29	0.53	0.41	1.13	0.27	0.24	1.44	0.86	0.59
	C6	(25)	0.80	0.28	0.35	0.69	0.16	0.23	0.97	0.73	0.75
	C7	(30)	1.65	0.72	0.44	1.59	0.38	0.24	2.13	0.74	0.35
	C8	(35)	1.17	0.42	0.36	0.86	0.20	0.24	1.03	0.69	0.67

The COVs of the S/E ratios for all eight previously proposed constitutive models range between 0.35 and 0.44 for infilled frames with $0 < f_m^{'} < 5$ MPa. The mean of the S/E ratios is closest to 1.00 for constitutive model C1 (mean = 0.93, COV = 0.38), which defines $F_{\max,m}$ as the product of the stress capacity of masonry prism and cross-sectional area of strut (see Table 1). The functional form for model C1 is based on fundamental principles of mechanics, and the model is able to simulate the peak strength of infilled RC frames rather well. Therefore, it is proposed to define parameter $F_{\max,m}$ as follows.

$$F_{\max,m} = \alpha_{\max,m} \times f_m^{'} b_m t_m \tag{39}$$

where $\alpha_{\max,m}$ is a factor depending on $f_m^{'}$, and other parameters were defined previously.

For $5 < f_m^{'} < 10$ MPa, model C1 led to the mean S/E ratio closest to 1.00 (mean = 0.99, COV = 0.25) among all models studied. It should be noted that all eight macro models led to COV between 0.23 and 0.26 for this range of $f_m^{'}$. Accordingly, Eq. (39) is also considered for $5 < f_m^{'} < 10$ MPa.

For $f_m^{'} > 10$ MPa, the least COV (= 0.35) is obtained through constitutive model C7, which defines F_2 in terms of the results obtained through the diagonal compression tests on masonry walls (see Table 1). It is easier to perform tests on masonry prism compared to masonry walls. The next lowest COV is obtained through constitutive model C1 (mean = 1.61, COV = 0.49). Given its simplicity, it is proposed to consider the expression of Eq. (39) also for $f_m^{'} > 10$ MPa. It should be noted that there are only 20 samples with $f_m^{'} > 10$ MPa, and more experimental results may enable the selection of a better functional form.

Parameter $\alpha_{\text{max,m}}$ was set equal to 1.1, 1.0 and 0.4 for $0 < f_m^{'} < 5$ MPa, $5 < f_m^{'} < 10$ MPa and $f_m^{'} > 10$ MPa in order to achieve the mean values of S/E ratios for F_2 (see Fig. 4) close to 1.0, respectively. The values of the coefficient suggest that approximately 100% (40%) of masonry strength is "utilized" towards the overall strength of an infilled RC frame for $f_m^{'}$ smaller (greater) than 10 MPa.

The approach described above can be appreciated through Fig. 6. Panel (a) of the figure presents the average simulated-to-experimental ratios for parameters F_1, K_1, F_2, D_2 and R_{PP} obtained using strut model S3 and the eight constitutive models described in Table 1 for $0 < f_m^{'} < 5$ MPa. Panels (b) and (c) of the figure present results for $5 < f_m^{'} < 10$ MPa and $f_m^{'} > 10$ MPa, respectively. Panels (d), (e) and (f) of the figure present the ratios for the three ranges of $f_m^{'}$, respectively, with $F_{\text{max,m}}$ defined using the proposed method, i.e., Eq. (39), and

other parameters defined using the respective expressions presented in Table 1. It can be seen from the figures that the average simulated-to-experimental ratio for F_2 is 1.0 (indicated using a red circle).

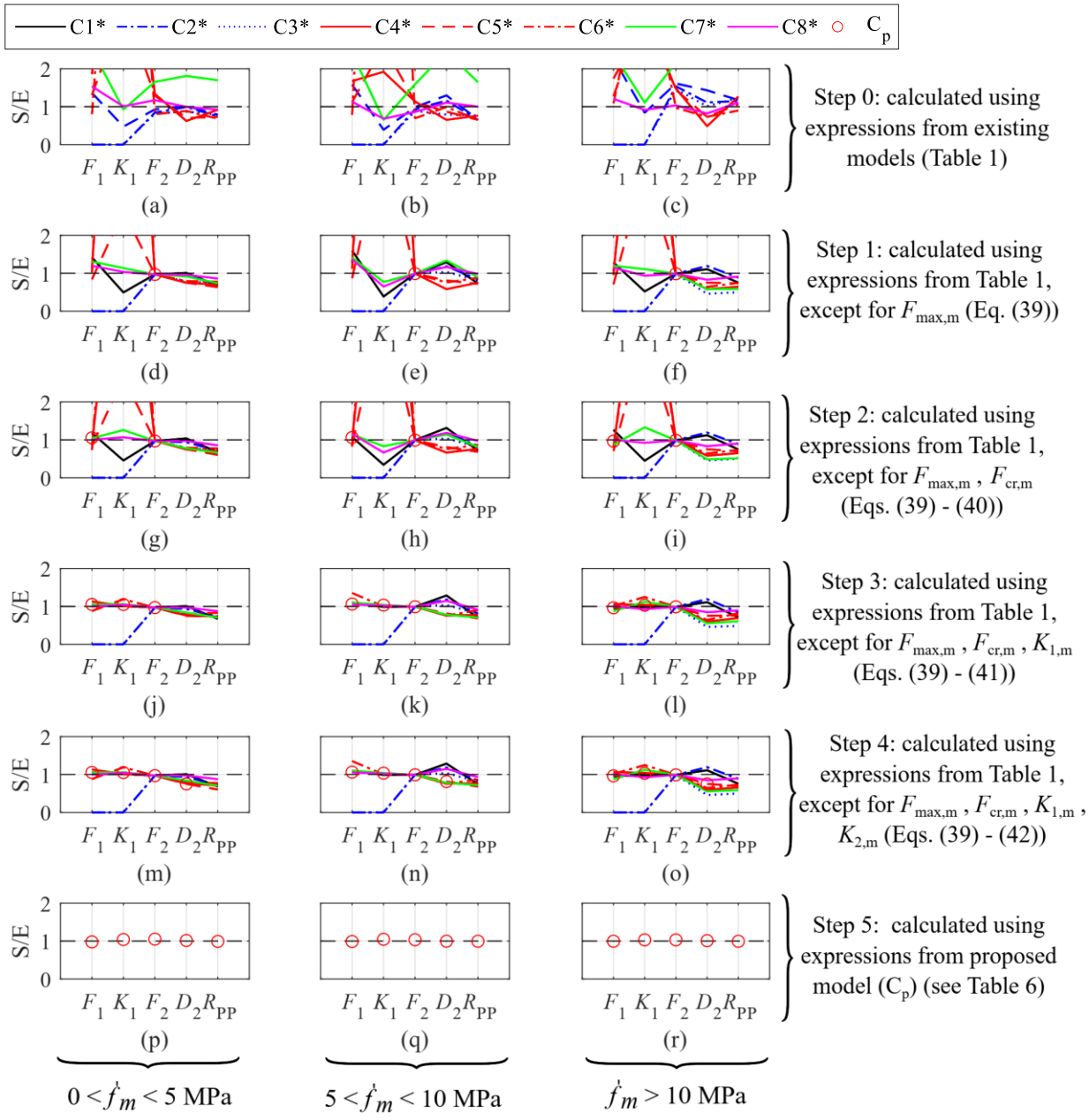

Fig. 6. Simulated-to-experimental ratios for parameters F_1, K_1, F_2, D_2 and R_{PP} at different steps of the development of the proposed model

6.1.2. Force corresponding to first major crack in masonry $\left(F_{cr,\mathrm{m}}\right)$

The next step was to characterize the force corresponding to the first major crack in masonry $F_{cr,\mathrm{m}}$ (see Fig. 5). For this part, $F_{\mathrm{max,m}}$ was given by Eq. (39) for all constitutive models, while other parameters of the models were defined using the expressions given in Table 1. Strut model S3 was used in combination with the variants of the eight constitutive models, and lateral force-deformation response of the 106 infilled RC frames (see Table 2) were simulated. The ratio of simulated force corresponding to the first major crack in infilled RC frame F_1 (see Fig. 4) to the corresponding experimental value (S/E) was determined for all 106 specimens. Notably, constitutive models C1, C4, C5, C6 and C8 consider $F_{cr,\mathrm{m}}$ equal to 0.75, 0.77, 0.60, 0.80 and 0.72 times $F_{\mathrm{max,m}}$, respectively. The mean S/E ratios for F_1 were closest to 1.00, when $F_{cr,\mathrm{m}}$ was set equal to $0.60\,F_{\mathrm{max,m}}$ (see [95]) irrespective of $f_m^{'}$. Accordingly, parameter $F_{cr,\mathrm{m}}$ is proposed to be defined as follows.

$$F_{cr,\mathrm{m}} = \alpha_{cr,\mathrm{m}} \times F_{\mathrm{max,m}} \tag{40}$$

where $\alpha_{cr,\mathrm{m}}$ is set equal to 0.60.

For different ranges of $f_m^{'}$, panels (g) through (i) of Fig. 6 present average simulated-to-experimental ratios for parameters F_1, K_1, F_2, D_2 and R_{PP} with $F_{\mathrm{max,m}}$ and $F_{cr,\mathrm{m}}$ defined using Eq. (39) and Eq. (40), respectively, and other parameters of the constitutive models defined using the expressions presented in Table 1. The average simulated-to-experimental ratios for parameters F_2 and F_1 are 1.0 (indicated using red circles).

6.1.3. Stiffness corresponding to first major point of cracking $\left(K_{1,\mathrm{m}}\right)$

With $F_{\max,\mathrm{m}}$ and $F_{cr,\mathrm{m}}$ defined using Eq. (39) and Eq. (40), respectively, the functional form for the initial axial stiffness of the masonry panel $K_{1,\mathrm{m}}$ (see Fig. 5) was established next. These definitions for the two parameters were used for all eight constitutive models, while the remaining parameters for the models were defined using the expressions presented in Table 1. In addition, a further variant of constitutive model C7 was considered, wherein the strut width parameter w in Eq. (29) was defined using Eq. (1) given by Mainstone [44] instead of $d_m/4$ as originally considered for C7. The lateral force-displacement response for all 106 specimens was computed using the nine macro models, and S/E ratios for the initial stiffness of infilled RC frames K_1 (see Fig. 4) were determined. Mean, STD and COV of these ratios obtained using the nine macro model are presented in Table 5. The variant of model C7 is denoted using C7M in the table.

Table 5. Mean simulated-to-experimental (S/E) ratios, corresponding standard deviations (STDs) and coefficients of variation (COVs) for initial stiffness of infilled RC frame

			$0 < f_m^{'} < 5$ MPa			$5 < f_m^{'} < 10$ MPa			$f_m^{'} > 10$ MPa		
Parameters	CM	Reference	Mean	STD	COV	Mean	STD	COV	Mean	STD	COV
$F_{max,m}$	$\alpha_{\max,\mathrm{m}} \times f_m^{'} b_m t_m$	Eq. (39)									
$F_{cr,m}$	$0.60 \times F_{\max,\mathrm{m}}$	Eq. (40)									
K_1	C1	Table 1	0.46	0.39	0.85	0.34	0.22	0.65	0.45	0.5	1.11
	C2	-	-	-		-	-		-	-	
	C3	-	-	-		-	-		-	-	
	C4	Eq. (15)	8.47	16.61	1.96	8.92	13.5	1.51	6.97	9.82	1.41
	C5	Eq. (21)	2.65	2.03	0.77	4.57	5.41	1.18	3.74	3.08	0.82
	C6	Eq. (24)	11.97	13.54	1.13	12.22	12.9	1.06	6.41	7.91	1.23
	C7	Eq. (29)	1.26	1.07	0.85	0.83	0.53	0.64	1.33	0.93	0.70
	C7M	Eq. (29), Eq. (1)	**0.64**	**0.48**	**0.75**	**0.39**	**0.21**	**0.54**	**0.64**	**0.37**	**0.58**
	C8	Eq. (34)	1.07	0.74	0.69	0.67	0.4	0.60	0.92	0.39	0.42

Model C8 led to the least COV for $0 < f_m^{'} < 5$ MPa among all the nine models studied (mean = 1.07, COV = 0.69). This model considers elastic modulus of masonry, and thickness, height and length of the masonry panel. The expression of model C8 is somewhat intuitive. The

next lowest COV was obtained using C7M model (mean = 0.64, COV = 0.75). This model considers a mechanics-based definition of axial stiffness. Considering its simplicity, it is proposed to define $K_{1,\mathrm{m}}$ based on the definition considered for constitutive model C7M.

$$K_{1,\mathrm{m}} = \alpha_{1,\mathrm{m}} \frac{E_m b_m t_m}{d_m} \tag{41}$$

where $\alpha_{1,\mathrm{m}}$ is a factor depending on $f_m^{'}$, and other parameters were defined previously. For $5 < f_m^{'} < 10$ MPa, the least COV was obtained for constitutive model C7M (mean = 0.39, COV = 0.54). Therefore, it was decided to consider the expression of Eq. (41) for this infill strength range as well. This expression was adopted also for $f_m^{'} > 10$ MPa because of its simplicity, despite model C8 leading to somewhat better simulation in terms of COV. Parameter $\alpha_{1,\mathrm{m}}$ was set equal to 1.8, 2.8 and 1.8 for $0 < f_m^{'} < 5$ MPa, $5 < f_m^{'} < 10$ MPa and $f_m^{'} > 10$ MPa in order to achieve the mean value of S/E ratio for K_1 (see Fig. 4) close to 1.0, respectively.

For different ranges of $f_m^{'}$, panels (j) through (l) of Fig. 6 present average simulated-to-experimental ratios for parameters F_1, K_1, F_2, D_2 and R_{PP} with $F_{\mathrm{max,m}}$, $F_{cr,\mathrm{m}}$ and $K_{1,\mathrm{m}}$ defined using Eqs. (39) through (41), respectively, and other constitutive model parameters defined using the expressions presented in Table 1. The average simulated-to-experimental ratios for parameters F_2, F_1 and K_1 are 1.0 (indicated using red circles).

6.1.4. Stiffness corresponding to peak strength $\left(K_{2,\mathrm{m}}\right)$

The next step was to establish the expression for the secant stiffness corresponding to peak strength of masonry strut $K_{2,\mathrm{m}}$ (see Fig. 5). Many constitutive models define $K_{2,\mathrm{m}}$ using the functional form considered for $K_{1,\mathrm{m}}$ (e.g., C2, C4, and C5). The same approach is adopted in the present study as well. Accordingly, $K_{2,\mathrm{m}}$ is defined as follows.

$$K_{2,\mathrm{m}} = \alpha_{2,\mathrm{m}} \times \frac{E_m b_m t_m}{d_m} \tag{42}$$

where $\alpha_{2,\mathrm{m}}$ is a function of $f_m^{'}$, and other parameters were defined previously. With $F_{\mathrm{max,m}}$, $F_{cr,\mathrm{m}}$ and $K_{1,\mathrm{m}}$ defined using Eq. (39), Eq. (40) and Eq. (41), respectively, parameter $\alpha_{2,\mathrm{m}}$ was set equal to 0.7, 1.3 and 0.5 for $0 < f_m^{'} < 5$ MPa, $5 < f_m^{'} < 10$ MPa and $f_m^{'} > 10$ MPa in order to achieve the mean value of S/E ratio for D_2 (see Fig. 4) close to 1.0, respectively.

For different ranges of $f_m^{'}$, panels (m) through (o) of Fig. 6 present the average simulated-to-experimental ratios for parameters F_1, K_1, F_2, D_2 and R_{PP} with $F_{\mathrm{max,m}}$, $F_{cr,\mathrm{m}}$, $K_{1,\mathrm{m}}$ and $K_{2,\mathrm{m}}$ defined using Eqs. (39) through (42), respectively, and the other parameters defined using the respective expressions presented in Table 1. The average ratio for parameters F_2, F_1 and K_1 is 1.0, while that for parameter D_2 is less than 1.0. The average ratio for parameter D_2 was found sensitive to the definitions of other post-peak constitutive model parameters.

6.1.5. Residual strength $\left(F_{res,\mathrm{m}}\right)$ and slope for the post-peak segment $\left(K_{3,\mathrm{m}}\right)$

Eqs. (39) through (42) define the proposed constitutive model for masonry strut up to peak strength. The post-peak behaviour is to be characterized using the slope for the post-peak segment $K_{3,\mathrm{m}}$ and residual strength $F_{res,m}$ (see Fig. 5). Parameter $K_{3,\mathrm{m}}$ can be defined using the functional form considered for $K_{1,\mathrm{m}}$ (e.g., C4, C6). Similarly, $F_{res,m}$ can be defined using the functional form for $F_{\mathrm{max,m}}$ (e.g., C1, C4, C6, C8). Thirty seven out of 106 infilled RC frames were considered to have been loaded till respective residual strengths (see [95]). Expressions for these two post-peak parameters are given below.

$$F_{res,\mathrm{m}} = \alpha_{res,\mathrm{m}} \times F_{\mathrm{max,m}} \tag{43}$$

$$K_{3,\mathrm{m}} = \alpha_{3,\mathrm{m}} \frac{E_m b_m t_m}{d_m} \tag{44}$$

where $\alpha_{res,\mathrm{m}}$ and $\alpha_{3,\mathrm{m}}$ are factors depending on $f_m^{'}$, and other parameters were defined previously. These two parameters were established together through iterations. The final value of parameter $\alpha_{3,\mathrm{m}}$ ($\alpha_{res,\mathrm{m}}$) was set equal to 0.09 (0.70), 0.08 (0.70) and 0.05 (0.70) for $0 < f_m^{'} < 5$ MPa, $5 < f_m^{'} < 10$ MPa and $f_m^{'} > 10$ MPa in order to achieve the value of post-peak response parameter R_{PP} (see Section 5) close to 1.0, respectively. It should be noted that the value of $\alpha_{res,\mathrm{m}}$ (= 0.70) is close to the average of the ratios of the residual to peak strength of infilled RC frames for the 37 specimens considered. Most constitutive models considered in the present study define the residual masonry strut strength in the range of 0 – 40% of the corresponding peak strength. Kumar et al. [43] among others note that a "weak" masonry would lead to a greater residual strength (e.g., 70% of the peak strength) for the infilled RC frames, and vice-versa. It should be noted that 73% of the 37 specimens considered to characterize the post-peak behaviour have $f_m^{'}$ smaller than 5 MPa.

For different ranges of $f_m^{'}$, panels (p) through (r) of Fig. 6 present the average simulated-to-experimental ratios for parameters F_1, K_1, F_2, D_2 and R_{PP} obtained using the proposed constitutive model, i.e., Eqs. (39) through (44). The average simulated-to-experimental ratio is 1.0 for all five backbone parameters.

A summary of the proposed masonry constitutive model corresponding to the S3 strut model is presented in Table 6. The steps to implement the model are outlined in Fig. 7. These steps can be extended to model multi-bay-multi-story infilled RC frames as well.

Table 6. Proposed masonry constitutive model (see Fig. 2 and Fig. 5)

Parameter	Expression	Multiplier		
		$0 < f_m^{'} < 5$ MPa	$5 < f_m^{'} < 10$ MPa	$f_m^{'} > 10$ MPa
$F_{\max,m}$	$\alpha_{\max,m} \times f_m^{'} b_m t_m$	$\alpha_{\max,m} = 1.1$	$\alpha_{\max,m} = 1.0$	$\alpha_{\max,m} = 0.4$
$F_{cr,m}$	$\alpha_{cr,m} \times \alpha_{\max,m} f_m^{'} b_m t_m$	$\alpha_{cr,m} = 0.6$	$\alpha_{cr,m} = 0.6$	$\alpha_{cr,m} = 0.6$
$K_{1,m}$	$\alpha_{1,m} \times \frac{E_m b_m t_m}{d_m}$	$\alpha_{1,m} = 1.8$	$\alpha_{1,m} = 2.8$	$\alpha_{1,m} = 1.8$
$K_{2,m}$	$\alpha_{2,m} \times \frac{E_m b_m t_m}{d_m}$	$\alpha_{2,m} = 0.7$	$\alpha_{2,m} = 1.3$	$\alpha_{2,m} = 0.5$
$F_{res,m}$	$\alpha_{res,m} \times \alpha_{\max,m} f_m^{'} b_m t_m$	$\alpha_{res,m} = 0.7$	$\alpha_{res,m} = 0.7$	$\alpha_{res,m} = 0.7$
$K_{3,m}$	$\alpha_{3,m} \times \frac{E_m b_m t_m}{d_m}$	$\alpha_{3,m} = 0.09$	$\alpha_{3,m} = 0.08$	$\alpha_{3,m} = 0.05$

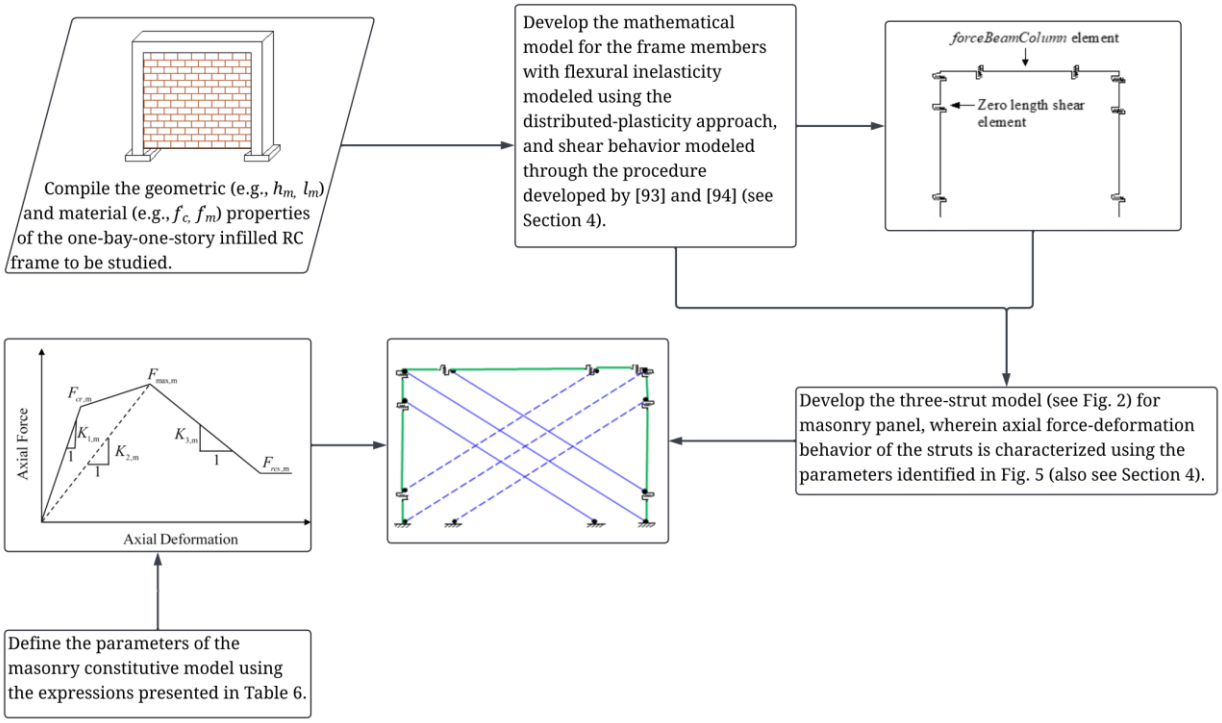

Fig. 7. Summary of procedure to use the proposed masonry constitutive model for analysis

6.2. Performance

This section presents a discussion on the performance of the proposed masonry constitutive model in simulating the response of one-bay-one-story, and multi-bay-multi-story infilled RC frames.

6.2.1. One-bay-one-story frames

This section presents the performance of the proposed constitutive model (along with models C1 through C8 developed in the past) in simulating the response of 106 experimentally studied infilled RC frames (see Table 2). Also discussed is the effectiveness of the proposed model in combination with single- and two-strut models. Further, it is examined whether the simulation is correlated with some key geometrical and material parameters of the frame and infills (e.g., stiffness of infill relative to frame). Finally, the relationship between the observed failure modes in the infilled RC frame and simulated backbone parameters is studied.

6.2.1.1 Simulation of backbone parameters

Influence of constitutive models

The proposed masonry constitutive model (denoted using CP in this section) was used in combination with strut model S3 to simulate the lateral force-displacement response of the 106 one-bay-one-story masonry-infilled RC frame specimens listed in Table 2. Fig. 8(a) presents the mean and mean ± standard deviation of the S/E ratios for the peak strength F_2 of infilled RC frames (see Fig. 4) for $0 < f_m^{'} < 5$ MPa. Results for the proposed model are highlighted using red circles. Also presented in the panel are the results for the previously proposed constitutive models C1 through C8 (see Table 1) in combination with strut model S3. Expectedly, the proposed model is able to simulate the peak strength considerably better compared to the previously proposed models. The next best simulation could be performed using model C1, which was developed using the experimental results for masonry prism without considering the interaction between frame and infill. This observation suggests that the influence of the frame-infill interaction on the peak strength of infilled RC frames is relatively small. Similar observations can be made for panel (b) of Fig. 8, which reports the results for $5 < f_m^{'} < 10$ MPa. It should be noted that the

mean ratios obtained using model C8 are greater than 1.0 for $0 < f_m^{'} < 5$ MPa, and smaller than 1.0 for $5 < f_m^{'} < 10$ MPa. However, performance of this model is similar to the proposed model for $f_m^{'} > 10$ MPa, as can be seen from Fig. 8(c).

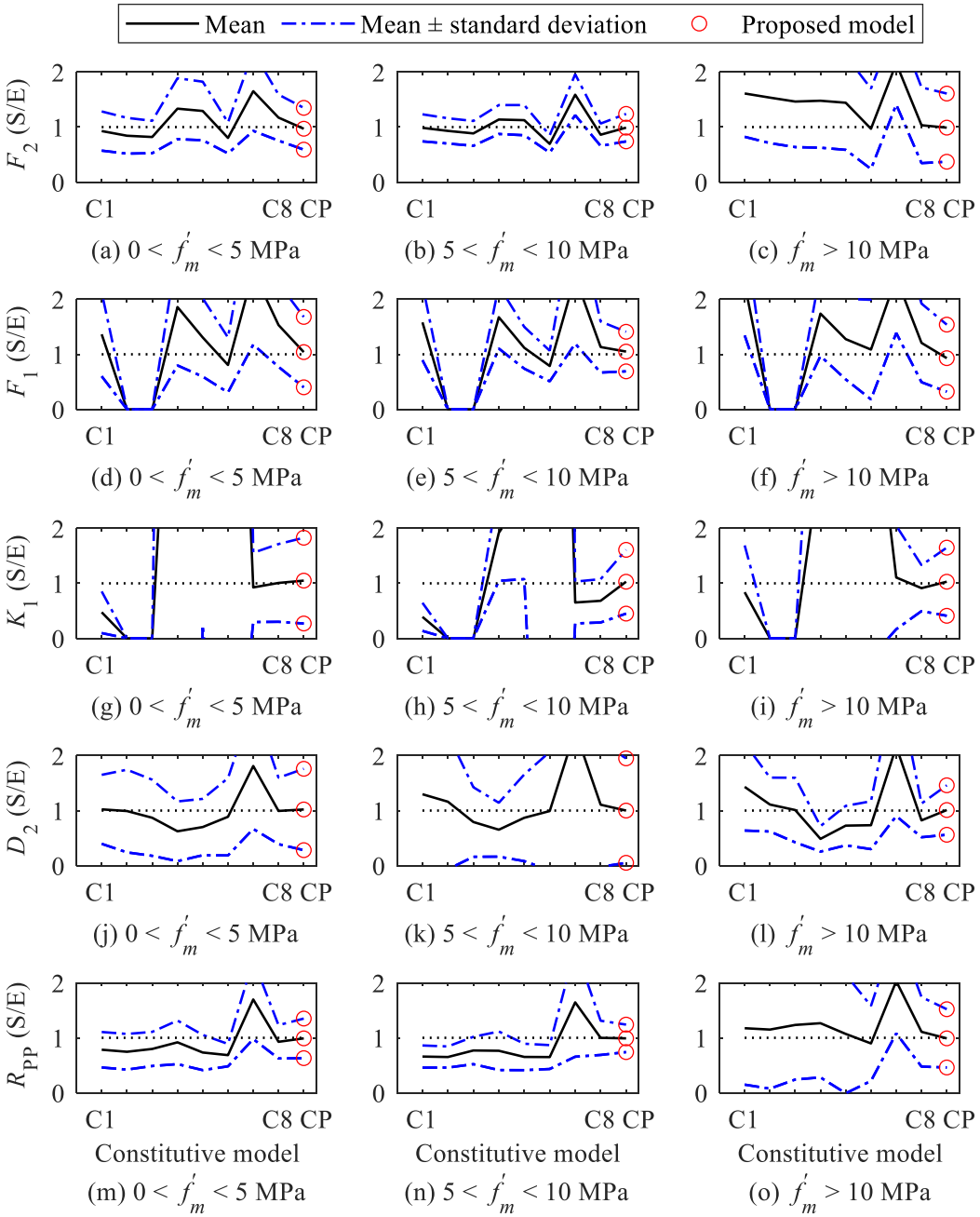

Fig. 8. Ratios of simulated-to-experimental (S/E) values of lateral force-displacement parameters (see Fig. 4) for the proposed and some existing constitutive models

Panels (d) through (f) of Fig. 8 present the S/E ratios for force corresponding to the first major crack in frame or infill F_1 (see Fig. 4) for the three ranges of infill strength, respectively. The

proposed model performs better compared to other constitutive models. Overall, a similar conclusion can be drawn for other parameters, namely, K_1, D_2 and R_{PP} (see Fig. 4), as can be seen from panels (g) through (o) of Fig. 8.

Influence of select strength and stiffness parameters

The proposed model was developed considering the data in three brackets based on masonry prism strength. Within each bracket, the influence of strength parameters for beam and columns, and ratio of masonry infill stiffness to that of frame are examined next. Accordingly, correlation coefficients between S/E ratios of backbone parameters (F_2, F_1, K_1, D_2 and R_{PP}) and each of the following parameters were calculated: (1) product of characteristic concrete strength and cross-section for column $f_c^{'}b_c d_c$, (2) product of characteristic concrete strength and cross-section for beams $f_c^{'}b_b d_b$, and (3) a representative stiffness of infill relative to frame. The third parameter was characterised as the ratio of lateral stiffness of masonry $\left(E_m b_m t_m / d_m\right)\cos^2(\theta)$ (e.g., [11]) to a representative lateral stiffness of frame EI_c / h^3 (e.g., [60]).

Fig. 9(a) presents the S/E ratios of F_2 corresponding to $f_c^{'}b_c d_c$. The correlation coefficients between the S/E ratios and $f_c^{'}b_c d_c$ is 0.04 for $0 < f_m^{'} < 5$ MPa, which can be considered small. For this range of masonry prism strength, the correlations are small also for parameters K_1, D_2 and R_{PP} (see panels (g), (j) and (m) of Fig. 9, respectively). However, the correlation for parameter F_1 is 0.23. For this range of $f_m^{'}$, correlation coefficients between the S/E ratios and $f_c^{'}b_b d_b$ are -0.08, 0.07, 0.04, -0.06 and -0.13 for parameters F_2, F_1, K_1, D_2 and R_{PP}, respectively (see panels (b), (e), (h), (k) and (n) of Fig. 9). Overall, the simulations of the backbone parameters

can be considered to be not meaningfully correlated with the strength of frame members for $0 < f_m^{'} < 5$ MPa.

For $5 < f_m^{'} < 10$ MPa, correlations between S/E ratios and $f_c^{'} b_c d_c$ ($f_c^{'} b_b d_b$) are 0.06, -0.09, - 0.31, 0.62 and 0.18 (0.11, -0.20, -0.20, 0.60 and 0.21) for parameters F_2, F_1, K_1, D_2 and R_{PP} , as can be seen from panels (a), (d), (g), (j) and (m) (panels (b), (e), (h), (k) and (n)) of Fig. 9, respectively. These correlations are -0.22, -0.35, 0.70, -0.26 and -0.17 (-0.23, -0.34, 0.04, -0.34 and -0.22) for $f_m^{'} > 10$ MPa as can be seen from corresponding panels of Fig. 9, respectively. The magnitude and signs of the correlation coefficient do not indicate a meaningful pattern of the simulation results affected by the strength of frame members. It should be noted that only 16% and 19% of 106 one-bay-one-story specimens had $5 < f_m^{'} < 10$ MPa and $f_m^{'} > 10$ MPa, respectively. Additional data may help understand the patterns better.

Correlations between S/E ratios for different backbone parameters and representative stiffness of infill relative to frame were studied (data presented in panels (c), (f), (i), (l) and (o) of Fig. 9). The magnitudes and signs of these correlations suggest that the overall simulation of the backbone parameters are not considerably dependent on the relative stiffness.

Influence of strut models

At times it is desirable to use simpler strut models (e.g., S1) for the purpose of simulating the lateral force-displacement response of the infilled RC frames. Therefore, the lateral force-displacement responses of the 106 specimens (see Table 2) were simulated using the proposed masonry constitutive model in combination with strut models S1, S2 and S3 (see Fig. 1). Corresponding S/E ratios for the backbone parameters (see Fig. 4) are presented in Fig. 10.

○ $0 < f_m^{'} < 5$ MPa ✳ $5 < f_m^{'} < 10$ MPa ◇ $f_m^{'} > 10$ MPa

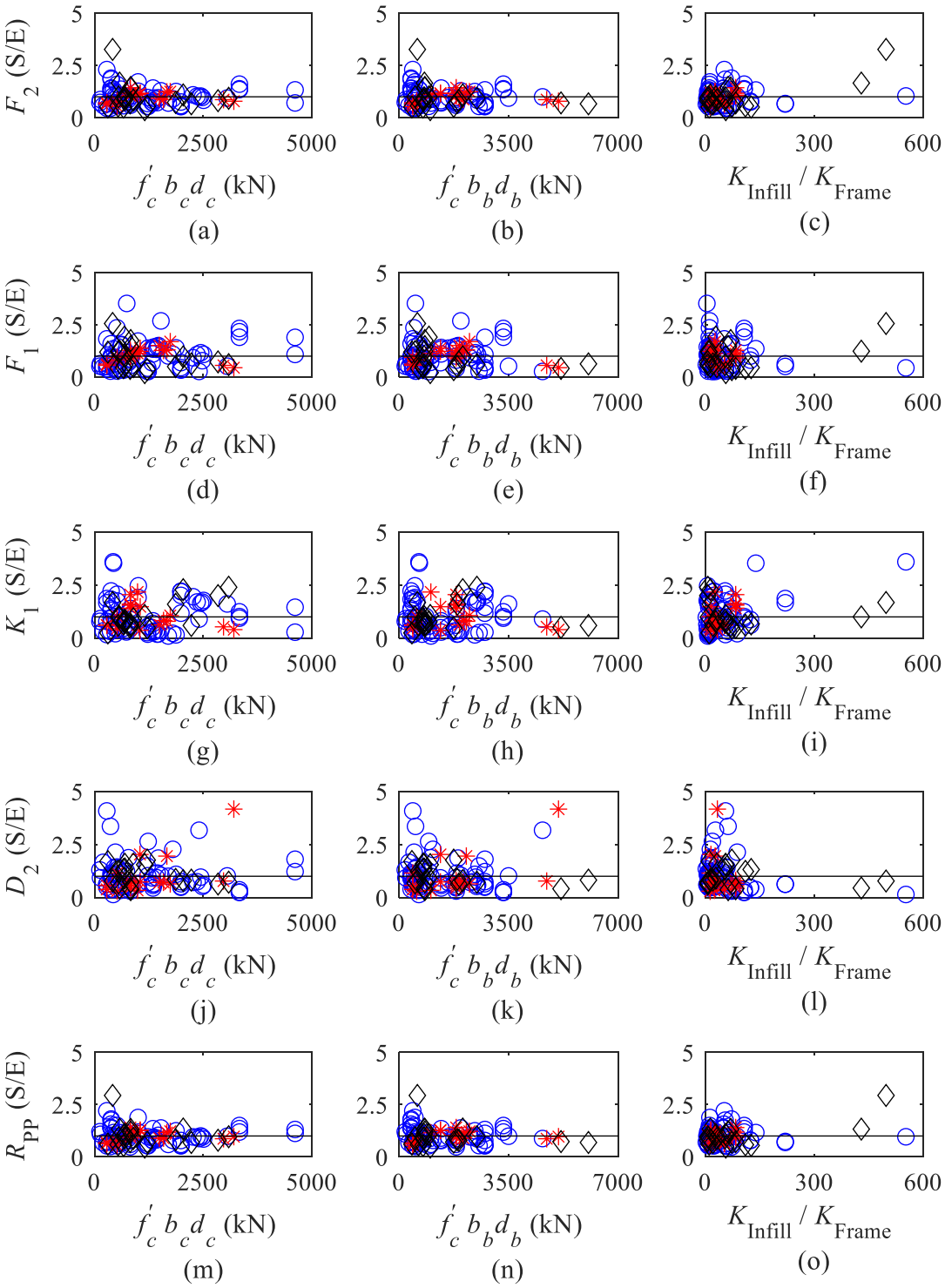

Fig. 9. Ratios of simulated-to-experimental (S/E) values of backbone parameters (see Fig. 4) plotted against different strength and stiffness parameters of the frame

1

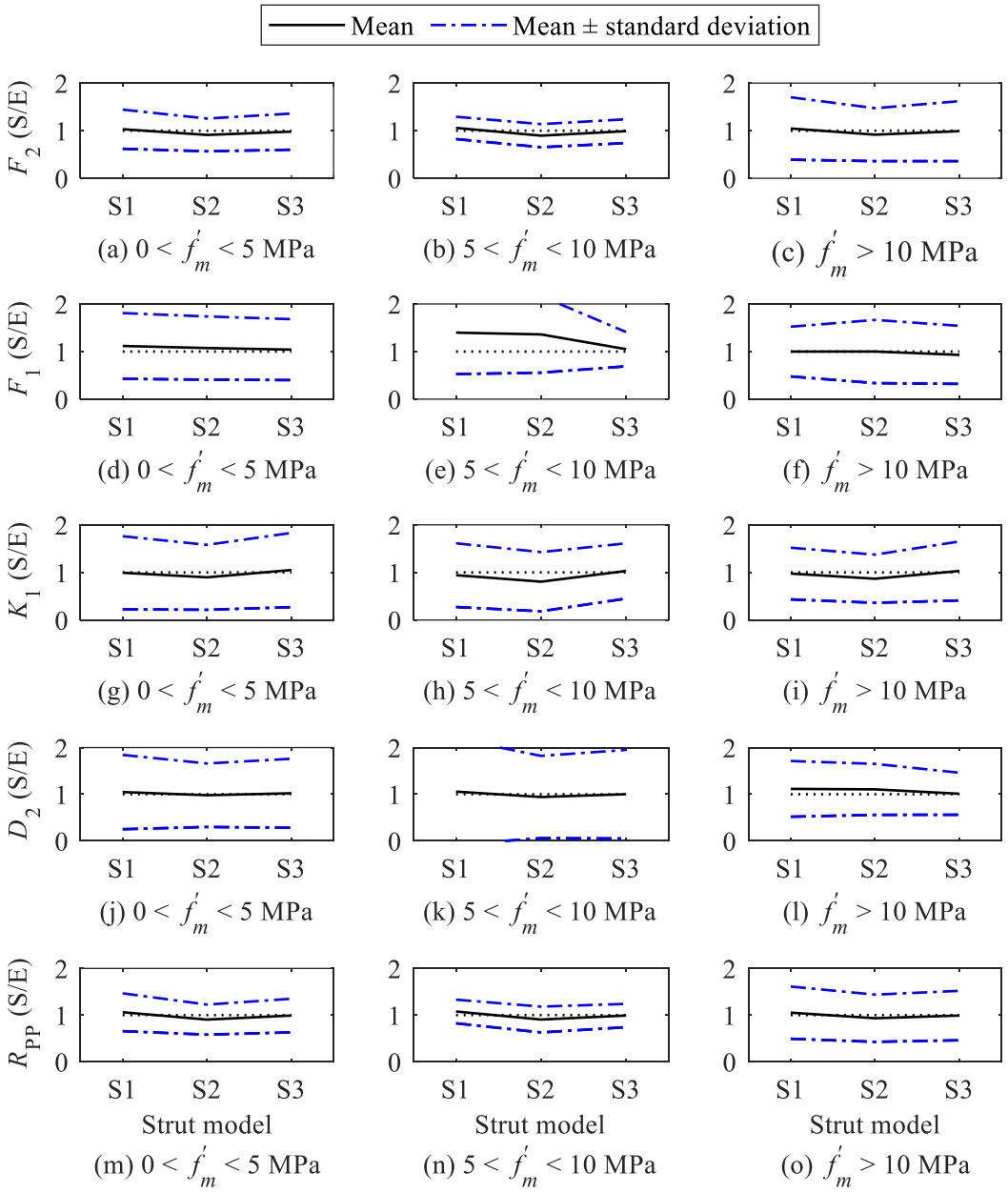

Fig. 10. Ratios of simulated-to-experimental (S/E) values of lateral force-displacement parameters (see Fig. 4) for the proposed constitutive model in combination with three strut models

The choice of strut model does not influence the simulation of the lateral force-displacement parameters for the masonry-infilled RC frames materially. However, the peak strength F_2 and initial stiffness K_1 obtained using that two-strut model are marginally smaller compared to single-strut and three-strut model, which can be attributed to additional deformation (and the

development of force) in the frame members close to the loaded corner due to the absence of a diagonal strut in the two-strut model.

Influence of observed failure mode in masonry panel

The proposed model did not consider the mode of failure in the masonry panel. However, it has been noted in the past that the response of the frame may depend significantly on the failure mode of infilled frames (e.g., [57], [60]). Out of 106 infilled frames considered herein, masonry panels underwent sliding shear, corner crushing and diagonal cracking failure in 42, 47 and 10 specimens, respectively; information on the remaining seven specimens was not available. Results simulated using S3-CP model for the 99 (= 42+47+10) specimens were considered further. The corresponding S/E ratios for parameters F_2 and R_{PP} were relatively close to 1.0 in case of sliding shear and corner crushing modes, while these were relatively close to 0.7 for diagonal cracking mode. Expectedly, K_1 was only marginally influenced by the mode of failure in masonry.

Further, the S/E ratios for different backbone parameters (see Fig. 4) were computed separately for specimens with reported shear (25 specimens) and flexural (49 specimens) failures in RC frame members. The ratios were close to 1.0 irrespective of the failure mode. Overall, it can be said that simulation of key response parameters for the infilled RC frames was not significantly influenced by the mode of failure in masonry (except when masonry failed in diagonal cracking mode, i.e., in approximately 10% specimens) or RC frame member.

6.2.1.2 Simulation of flexural and shear failure in frame members

Fig. 11(a) presents the comparison of simulated and observed instances of flexural failure in frame members for the infilled RC frames (see Section 5). The proposed model (S3-CP; indicated using S3 in the figure) was able to capture flexural failure (or its absence) correctly in 65 out of

74 infilled RC frame specimens for which flexure and/or shear failure was reported. The influence of the choice of strut model was marginal. Results for shear failure are reported in Fig. 11(b). The proposed model could capture shear failure (or its absence) in frame members for 57 out of the 74 specimens. Strut model S1 could lead to the correct or incorrect simulation of shear failure in frame members only in five out of the 74 specimens

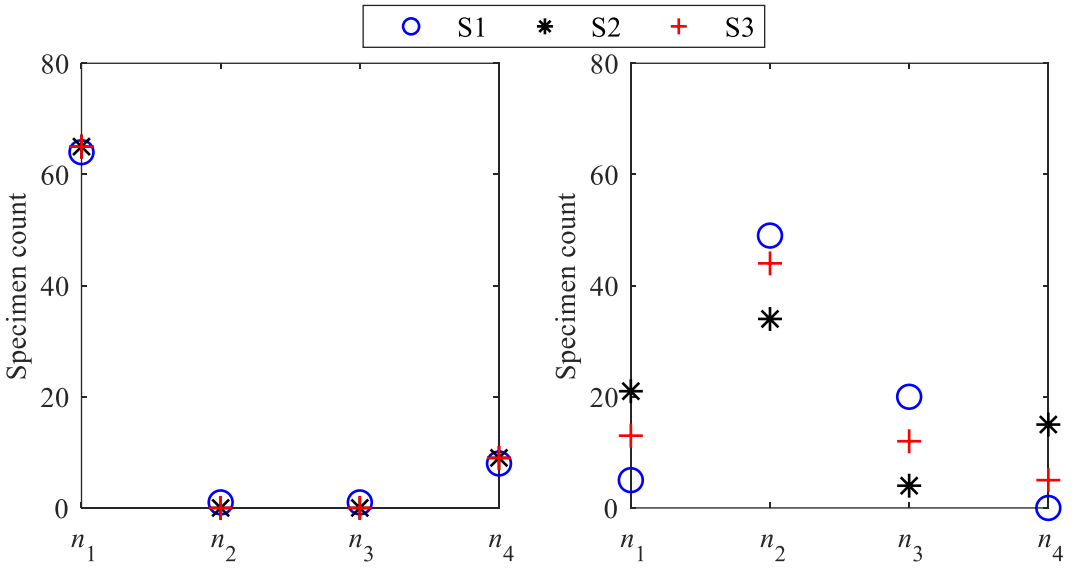

Fig. 11. Occurrence of (a) Flexure and (b) Shear failure in frame members ($n_1 \equiv$ experimentally observed and simulated, $n_2 \equiv$ experimentally not observed and not simulated, $n_3 \equiv$ experimentally observed and not simulated, $n_4 \equiv$ experimentally not observed and simulated)

6.2.2. Multi-bay-multi-story frames

The proposed macro model was used to compute the lateral force-displacement response of four multi-bay-multi-story infilled RC frames studied in the past. A one-bay-two-story (2S-1B) and a two-bay-one-story (1S-2B) frames experimentally studied by Suzuki et al. [96], a three-story-one-bay (3S-1B) frame experimentally studied by Koutas et al. [97], and a three-story-three-bay (3S-3B) frame experimentally studied by Dukuze and Dawe [98] were considered. Fig. 12 presents the experimentally obtained lateral force-displacement response of the frames along with that computed using the proposed macro model (S3-CP). Select details of the specimens are also specified in the figure. The proposed model could capture the response for specimens 2S-1B, 1S-2B and 3S-1B. The initial stiffness of the 3S-3B specimen also could

be captured well. However, simulated peak strength was substantially lower than the corresponding peak value. Accordingly, the overall simulation was inadequate for the specimen. It should be noted that $f_m^{'}$ for specimen 3S-3B was 39.6 MPa, which is beyond the range of $f_m^{'}$ considered to develop the constitutive model, i.e., 0.8 MPa – 26.7 MPa.

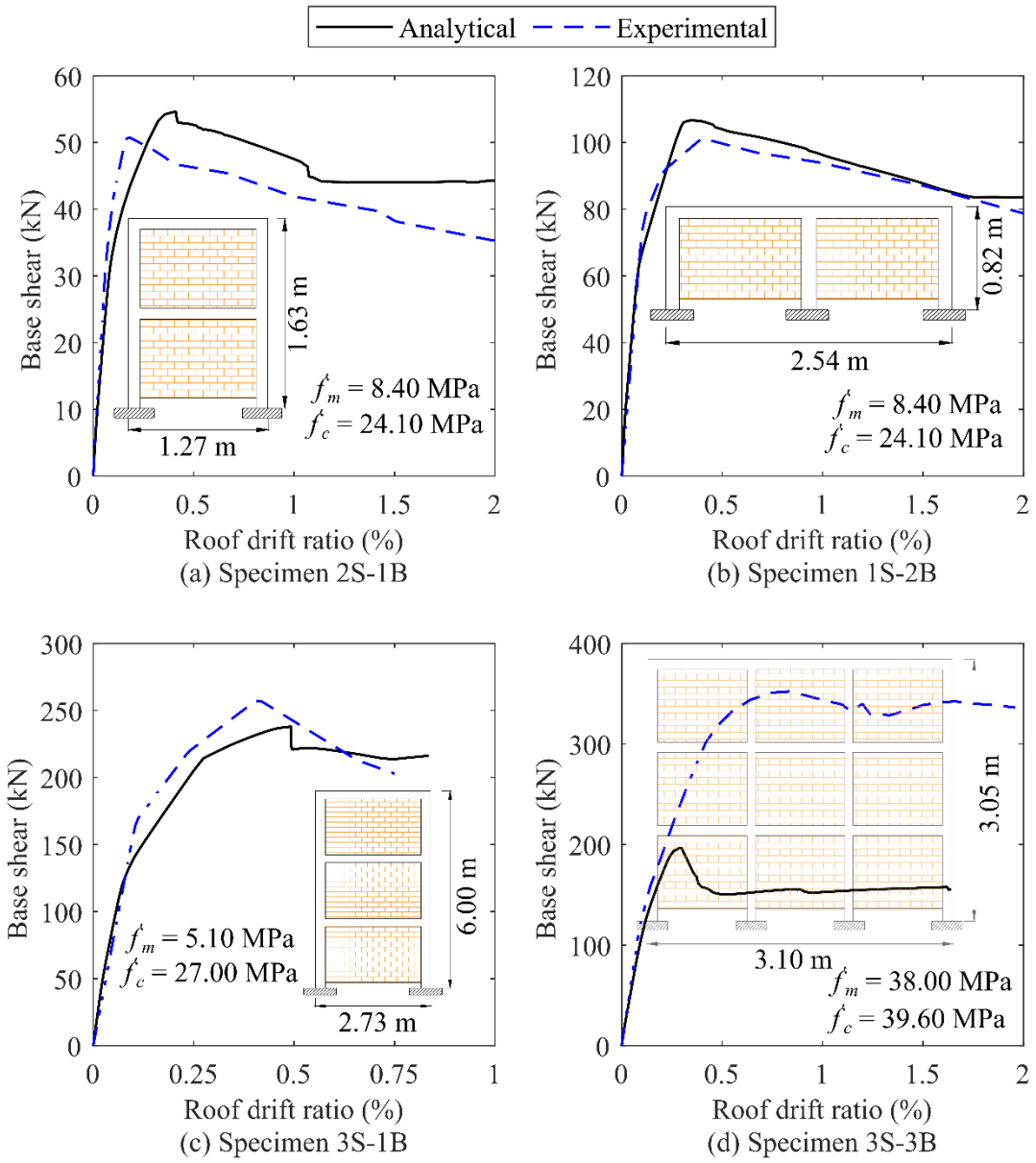

Fig. 12. Comparison of the simulated and experimentally obtained force-displacement responses using the proposed constitutive model

7. Limitations of the proposed model

The first limitation of the model is that it captures only the in-plane response of infilled frames. As noted previously, the masonry infill panels are vulnerable also to out-of-plane toppling (e.g., [19], [99]-[102]), particularly in the upper stories of a building. As an example, Fig. 13 shows in-plane failure of masonry panels in the lower as well as upper stories, and out-of-plane failure of the panels primarily in the upper stories. Masonry is expected to resist lateral loads through in-plane actions, particularly in the lower stories of the buildings. Consequently, the proposed model is expected to be useful in calculating global responses, for example, maximum forces generated in a building during an earthquake, inter-story drift ratio in the ground story, and risk of collapse. The model is also expected to be useful if masonry walls are restrained against out-of-plane failure. However, the model will need to be updated if combined effect of out-of-plane and in-plane response of masonry panel is to be simulated (e.g., [103] - [105]).

(a) In-plane damage [102] (b) In-plane and out-of-plane damages [9]

Fig. 13. Damages to masonry infill walls observed during past earthquakes

A yet another limitation of the proposed model is that it does not consider the effect of openings in the masonry infill wall. The openings are commonly provided to enable the passage of ducts, windows and doors. Presence of the openings is known to influence the response of infilled frames during earthquakes depending on position, size and type of openings (e.g., [12], [14], [15], [18]). The proposed model will need to be updated to account for these effects.

The proposed model has been developed considering the experimental results for 106 one-bay-one-story infilled RC frame specimens, and these very results have also been used for validation. Ideally, a fraction of these results should have been used for development, and remaining for validation. However, the size of the available database is small, particularly if individual ranges of masonry prism strength (e.g., $5 < f_m^{'} < 10$ MPa) are considered. Therefore, it was decided to use all 106 specimens for development as well as validation. This approach is in line with that taken for all constitutive models considered herein, namely, C1 through C8, which were developed as well as validated based on the entire dataset available with the team. Further, the proposed model was validated also against four multi-bay-multi-story infilled RC frames.

Finally, the model was developed using the available experimental data. The ranges of different parameters (e.g., height of specimens, masonry prism strength) are specified in Section 3. The coefficients in the proposed model may need to be updated as more data becomes available, particularly for specimens beyond the range considered herein.

8. Summary and conclusions

This paper presents an evaluation of the eight macro models in simulating the lateral force-displacement response of 106 one-bay-one-story reinforced concrete frames with masonry infill. Frame members were modelled using line elements capable of capturing flexural and shear failures, and interaction between axial loads and bending moment. Masonry was represented

using three parallel struts. The constitutive behavior of the struts was defined using eight existing models that were based on mechanics, semi-empirical, or empirical. The simulated response of the frames up to peak strength was compared with experimental results in terms of peak strength and corresponding secant stiffness, and strength corresponding to the first major crack in frame or infill and corresponding stiffness. Further, the average of ratios of simulated to experimental values of forces at different displacements was considered to characterize the simulation in the post-peak range. A new constitutive model was developed, and its performance was evaluated. Major observations and conclusions of the study are as follows.

(1) The dataset of 106 experimentally studied specimens had 69, 17 and 20 specimens with masonry prism strength ranging between 0 – 5 MPa, 5 – 10 MPa, and 10 – 27 MPa. Recognizing that the available data may not be representative of the population and that the means to account for the "missing" information may be limited, it was decided to perform the evaluation separately for the three ranges of masonry prism strength.

(2) Eight masonry constitutive models proposed in the past were evaluated. These models considered a range of expressions to characterize the model parameters. Expressions based on fundamental principles of mechanics could lead to minimum (or close to minimum) coefficient of variation for the simulated-to-experimental ratios of relevant backbone parameters of masonry-infilled RC frames.

(3) A new masonry constitutive model was proposed wherein all strength parameters were defined as a factor multiplied by the product of masonry prism strength and the area of diagonal strut representing masonry. Further, all stiffness parameters of the model were defined as a factor multiplied by the product of elastic modulus of masonry multiplied by the area of strut divided by the diagonal length of masonry panel. The factors were calibrated up to one significant figure for the three ranges of masonry prism strength.

(4) The peak lateral strength of infilled frames could be captured effectively using the proposed constitutive model, which explicitly considered the interaction between frame and infill. This model is very similar to one proposed in the past, which was developed based on the experimental results for 84 masonry prisms (with strength less than 10 MPa) without considering the frame-infill interaction. Accordingly, it can be said that the consideration of frame-infill interaction does not materially influence the lateral force-displacement response of infilled RC frames for masonry prism strength less than 10 MPa.

(5) In comparison with previously proposed masonry constitutive models, the proposed model could simulate the response of 106 one-bay-one-story infilled RC frames with effectively, despite its simplicity. The model was also shown to simulate the lateral response of three multi-bay-multi-story infilled RC frames. However, the model could not perform well for a multi-bay-multi-story frame with a rather high masonry prism strength. The model is expected to be useful in practical designs, and seismic performance assessment of a class of infilled RC frame buildings.

(6) Correlation coefficients between simulated-to-experimental ratios of backbone parameters of infilled frames and strength parameters for RC frame members were either small or had different signs for the three ranges of masonry prism strength, implying that the strength of response calculation was not materially affected by the strength parameters for frame members. A similar observation was made for stiffness of masonry panel relative to RC frame.

(7) The average simulated-to-experimental ratio of peak strength of infilled RC frame was close to 1.0 irrespective of whether shear or flexural failure was observed in the frame members. A similar observation was made regarding the shear sliding and corner crushing model of failure in masonry panel.

(8) Influence of the choice of the strut model was small in simulating the lateral force-displacement response, which further suggests that consideration of frame-infill interaction does not substantially affect the lateral force-displacement response calculation for infilled RC frames. Accordingly, the proposed constitutive models can be used in combination with single- or two-strut models. The single-strut model should not be used if capturing the shear failure in frame members is important.

Acknowledgements

Financial support was provided by Science and Engineering Research Board (File No. YSS/2015/1514) of Department of Science and Technology, Government of India.

References

[1] Gunay MS, Mosalam KM. Structural Engineering Reconnaissance of the April 6, 2009, Abruzzo, Italy, Earthquake, and Lessons Learned. PEER Report 2010/105, Pacific Earthquake Engineering Research Center, College of Engineering, University of California, Berkeley; 2010.

[2] Sezen H, Elwood JK, Whittaker SA, Mosalam MK, Wallace WJ, Stanton FJ. Structural Engineering Reconnaissance of the August 17, 1999, Kocaeli (Izmit), Turkey, Earthquake. PEER Report 2000/09, Pacific Earthquake Engineering Research Center, College of Engineering, University of California, Berkeley; 2000.

[3] Earthquake Engineering Research Institute. Learning from earthquakes: The M_w 7.6 Aquila, Michoacan, Mexico, Earthquake of September 19, 2022. EERI Special Earthquake Report, September, EERI, Oakland, CA; 2009.

[4] Earthquake Engineering Research Institute. Learning from earthquakes: The M_w 6.4 Durres, Albania, Earthquake of November 26, 2019. EERI Special Earthquake Report, January, EERI, Oakland, CA; 2022.

[5] Lee GC, Loh CH. The Chi-Chi, Taiwan Earthquake of September 21, 1999: Reconnaissance Report. Technical Report MCEER-00-0003, University at Buffalo, State University of New York, Buffalo, NY; 2000.

[6] Ricci P, de Luca F, Verderame GM. 6th April 2009 L'Aquila earthquake, Italy: Reinforced concrete building performance. Bull Earthq Eng 2011;9:285–305.

[7] Abrahamczyk L, Penava D, Markušić S, Stanko D, Luqman HP, Haweyou M, Schwarz, J. Die Magnitude 6.4 Albanien und Kroatien Erdbeben Ingenieuranalyse der Erdbebenschäden und Erfahrungswerte für die Baunormung. Bautechnik (Berlin, West. 1984), 99 (2022), 1; 18-30.

[8] Gur T, Pay AC, Ramirez JA, Sozen MA, Johnson AM, Irfanoglu A, et al. Performance of school buildings in Turkiye during the 1999 düzce and the 2003 bingöl earthquakes. Earthq Spectra 2009;25:239–56.

[9] Earthquake Engineering Research Institute. Learning from earthquakes: The M_w 7.8 Kahramanmaraş, Turkiye, Syria, Earthquake of February 6th, 2023. EERI Special Earthquake Report, May, EERI, Oakland, CA; 2023

[10] Klingner RE, Bertero VV. Earthquake resistance of infilled frames. J Struct Div 1978; 104(6):973-89.

[11] Paulay T, Priestley MJN. Seismic design of reinforced concrete and masonry buildings. New York: John Wiley; 1992.

[12] Sigmund V, Penava D. Influence of openings, with and without confinement, on cyclic response of infilled R-C frames - An experimental study. J Earthq Eng 2014;18:113–46

[13] Pradhan, B, Zizzo M; Sucato V, Cavaleri L, Penava D, Anić F, Sarhosis V. A macro-element modelling technique to account for IP and OOP interactions in URM infilled RC or steel building. Brick and Block Masonry - From Historical to Sustainable Masonry. London : Delhi: CRC Press, 2020. 9.

[14] Di Trapani F, Khan NA, Zhou L, Demartino C, Monti G. Cyclic response of infilled RC frames with window and door openings: Experimental results and damage interpretation. Earthq Eng Struct Dyn 2024;53:43–67.

[15] Anić F, Penava D, Abrahamczyk L, Sarhosis V. On the mechanical behaviour of masonry infilled RC frames, with and without openings, subjected to simultaneous in-plane (IP) and out-of-plane (OoP) loading. Bull Earthq Eng 2023.

[16] Rodrigues H, Varum H, Costa A. Simplified macro-model for infill masonry panels. J Earthq Eng 2010;14:390–416.

[17] Al Hanoun MH, Abrahamczyk L, Schwarz J. Macromodeling of in- and out-of-plane behavior of unreinforced masonry infill walls. Bull Earthq Eng 2019;17:519–35.

[18] Penava D, Sarhosis V, Kožar I, Guljaš I. Contribution of RC columns and masonry wall to the shear resistance of masonry infilled RC frames containing different in size window and door openings. Eng Struct 2018;172:105–30.

[19] Anić F, Penava D, Abrahamczyk L, Sarhosis V. A review of experimental and analytical studies on the out-of-plane behaviour of masonry infilled frames. Bull Earthq Eng 2011;18: 2191–2246.

[20] Stavridis A, Shing PB. Finite-Element Modeling of Nonlinear Behavior of Masonry-Infilled RC Frames. J Struct Eng 2010;136:285–96.

[21] Mohyeddin A, Goldsworthy HM, Gad EF. FE modelling of RC frames with masonry infill panels under in-plane and out-of-plane loading. Eng Struct 2013;51:73–87.

[22] Allouzi R, Irfanoglu A, Haikal G. Non-linear finite element modeling of RC frame-masonry wall interaction under cyclic loadings. In: 10th US National Conference on Earthquake Engineering, Anchorage, United States of America; 2014.

[23] Dhir PK, Tubaldi E, Ahmadi H, Gough J. Numerical modelling of reinforced concrete frames with masonry infills and rubber joints. Eng Struct 2021;246.

[24] Jeon JS, Park JH, DesRoches R. Seismic fragility of lightly reinforced concrete frames with masonry infills. Earthq Eng Struct Dyn 2015; 44(11):1783–1803.

[25] Bureau of Indian standards (BIS). Indian standard criteria for earthquake resistant design of structures. Part 1: General provisions and buildings, Standard IS 1893, Part 1, Bureau of Indian Standards, New Delhi, India; 2016.

[26] Federal Emergency Management Agency (FEMA). Evaluation of earthquake damaged concrete and masonry wall buildings, Report FEMA 306, Federal Emergency Management Agency, Washington, DC; 2000.

[27] Sattar S, Liel AB. Seismic performance of nonductile reinforced concrete frames with masonry infill walls - II: Collapse assessment. Earthq Spectra 2016; 32:819–42.

[28] El-Dakhakhni WW, Elgaaly M, Hamid AA. Three-strut model for concrete masonry-infilled steel frames. J Struct Eng 2003; 129:177–85.

[29] Huang H, Burton HV, Sattar S. Development and utilization of a database of infilled frame experiments for numerical modeling. J Struct Eng 2020; 146:04020079.

[30] Panagiotakos TB, Fardis MN. Seismic response of infilled RC frames structures. In: 11th World Conference on Earthquake Engineering, Acapulco, Mexico; 1996.

[31] Burton H, Deierlein G. Simulation of seismic collapse in nonductile reinforced concrete frame buildings with masonry infills. J Struct Eng 2014; 140:1–10.

[32] Kaushik HB, Rai DC, Jain SK. Uniaxial compressive stress-strain model for clay brick masonry. Curr Sci 2007; 92:497–501.

[33] Decanini L, Maollaioli F, Mura A, Saragoni R. Seismic performance of masonry infilled R/C frames. In: 13th World Conference on Earthquake Engineering, Vancouver, Canada; 2004.

[34] Huang H, Burton HV. A database of test results from steel and reinforced concrete infilled frame experiments. Earthq Spectra 2020; 36:1525–48.

[35] Asteris PG, Antoniou ST, Sophianopoulos DS, Chrysostomou CZ. Mathematical macromodeling of infilled frames: State of the art. J Struct Eng 2011; 137:1508–17.

[36] Mohyeddin A, Dorji S, Gad EF, Goldsworthy HM. Inherent limitations and alternative to conventional equivalent strut models for masonry infill-frames. Eng Struct 2017; 141:666–75.

[37] Ghosh R, Kumar M. Evaluation of macro models for masonry-infilled reinforced concrete frames. In: 13th North American Masonry Conference, Salt Lake City, United States of America; 2019.

[38] Han SW, Lee CS. Cyclic behavior of lightly reinforced concrete moment frames with partial- and full-height masonry walls. Earthq Spectra 2020; 36:599–628.

[39] Chrysostomou CZ. Effects of degrading infill walls on the nonlinear seismic response of two-dimensional steel frames. PhD Thesis. Cornell University Ithaca; 1991.

[40] Kaushik HB, Rai DC, Jain SK. Effectiveness of Some strengthening options for masonry-infilled RC frames with open first story. J Struct Eng 2009; 135:925–37.

[41] Noh NM, Liberatore L, Mollaioli F, Tesfamariam S. Modelling of masonry infilled RC frames subjected to cyclic loads: State of the art review and modelling with OpenSees. Eng Struct 2017; 150:599–621.

[42] Sharma M, Singh Y, Burton HV. Parametric study on the collapse probability of modern reinforced concrete frames with infills. Earthq Spectra 2023; 39:772–98.

[43] Kumar M, Rai DC, Jain SK. Ductility reduction factors for masonry-Infilled reinforced concrete frames. Earthq Spectra 2015; 31:339–65.

[44] Mainstone RJ. Supplementary note on the stiffness and strength of infilled frames. Build. Res. Establishment, London, England; 1974.

[45] Federal Emergency Management Agency (FEMA). NEHRP commentary on the guidelines for the seismic rehabilitation of buildings, Report FEMA 274, Federal Emergency Management Agency, Washington, DC; 1997.

[46] Smith BS, Carter C. A method of analysis for infilled frames. Proc Inst Civ Eng 1969; 44(1):31–48.

[47] Dolšek M, Fajfar P. The effect of masonry infills on the seismic response of a four storey reinforced concrete frame - a deterministic assessment. Eng Struct 2008; 30:1991–2001.

[48] Saneinejad A, Hobbs B. Inelastic design of infilled frames. J Struct Eng, 1995; 121(4):634–50.

[49] Smith BS. Behavior of square infilled frames. J Struct Div 1966; 92(1): 381–404.

[50] Colangelo F. Pseudo-dynamic seismic response of reinforced concrete frames infilled with non-structural brick masonry. Earthq Eng Struct Dyn 2005; 34:1219–41.

[51] Jain SK, Mitra K, Kumar M, Shah M. A proposed rapid visual screening procedure for seismic evaluation of RC-frame buildings in India. Earthq Spectra 2010; 26:709–29.

[52] Angel R, Abrams DP, Shapiro D, Uzarski J, Webster M. Behavior of reinforced concrete frames with masonry infills. Civil Engineering Studies, Structural Research Series No. 589, University of Illinois; 2009.

[53] Chiou TC, Hwang SJ. Tests on cyclic behavior of reinforced concrete frames with brick infill. Earthq Eng Struct Dyn 2015; 44(12):1939-1958.

[54] Porto FD, Guidi G, Benetta MD, Verlato N. Combined in-plane/out-of-plane experimental behaviour of reinforced and strengthened infill masonry walls. In: 12th Canadian Masonry Symposium, Vancouver, Canada; 2013.

[55] Combescure D, Pires F, Cerqueira P, Pegon P. Test on masonry infilled RC frames and its numerical interpretation. In: 11th World Conference on Earthquake Engineering, Acapulco, Mexico; 1996.

[56] Waly AA. Experimental and analytical work on the seismic performance of different types of masonry infilled reinforced concrete frames under cyclic loading. Ph.D. Thesis. Dokuz Eylül University, Izmir; 2010.

[57] Al-Chaar G, Issa M, Sweeney S. Behavior of masonry-infilled nonductile reinforced concrete frames. J Struct Eng 2002; 128:1055–63.

[58] Alwashali H, Torihata Y, Jin K, Maeda M. Experimental observations on the in-plane behaviour of masonry wall infilled RC frames; focusing on deformation limits and backbone curve. Bull Earthq Eng 2018; 16:1373–97.

[59] Cai G, Su Q. Effect of infills on seismic performance of reinforced concrete frame structures–A full-scale experimental study. J Earthq Eng 2019; 23:1531–59.

[60] Mehrabi AB, Shing PB, Schuller MP, Noland JL. Experimental evaluation of masonry-infilled RC frames. J of Struct Eng 1966; 122(3): 228–237.

[61] Basha SH, Kaushik HB. Behavior and failure mechanisms of masonry-infilled RC frames (in low-rise buildings) subject to lateral loading. Eng Struct 2016; 111:233–45.

[62] Kakaletsis DJ, Karayannis CG. Influence of masonry strength and openings on infilled R/C frames under cycling loading. J Earthq Eng 2008; 12:197–221.

[63] Combescure D, Pegon P. Application of the local-to-global approach to the study of infilled frame structures under seismic loading. Nucl Eng Des 2000; 196:17–40.

[64] Blackard B, Willam K, Mettupalayam S. Experimental observations of masonry infilled reinforced concrete frames with openings. Am Concr Institute, ACI Spec Publ 2009:199–221.

[65] Dautaj AD, Kadiri Q, Kabashi N. Experimental study on the contribution of masonry infill in the behavior of RC frame under seismic loading. Eng Struct 2018;165:27–37.

[66] Gazić G, Sigmund V. Cyclic testing of single-span weak frames with masonry infill. Građevinar 2016; 68(08):617-633.

[67] Bergami AV, Nuti C. Experimental tests and global modeling of masonry infilled frames. Earthq Struct 2015; 9:281–303.

[68] Mansouri A, Marefat MS, Khanmohammadi M. Experimental evaluation of seismic performance of low-shear strength masonry infills with openings in reinforced concrete frames with deficient seismic details. Struct Des Tall Spec Build 2011; 24:421–39.

[69] Misir IS, Ozcelik O, Girgin SC, Yucel U. The behavior of infill walls in RC frames under combined bidirectional loading. J Earthq Eng 2016; 20:559–86.

[70] Morandi P, Hak S, Magenes G. In-plane experimental response of strong masonry infills. In: 9th International Masonry Conference, Guimarães, Portugal; 2014.

[71] Tizapa SS. Experimental and numerical study of confined masonry walls under in-plane loads: Case: Guerrero State (Mexico). Ph.D. Thesis. Université Paris-Est, Paris; 2009.

[72] Verderame GM, Ricci P, Gaudio CD, Risi MTD. Experimental tests on masonry infilled gravity and seismic-load designed RC frames. In:16th International Brick Block Masonry Conference, Padova, Italy; 2016.

[73] Akhound F, Vasconcelos G, Lourenço PB, Palha C, Silva L. In-plane and out-of plane experimental characterization of RC masonry infilled frames. In: 6th International Conference on Mechanics and Materials in Design, Azores, Portugal; 2015.

[74] Zovkic J, Sigmund V, Guljas I. Cyclic testing of a single bay reinforced concrete frames with various types of masonry infill. Earthq Eng Struct Dyn 2013; 42(8):1131-1149.

[75] Kumar M, Haider M, Lodi SH. Response of low-quality solid concrete block infilled frames. Proc Inst Civ Eng Struct Build 2016; 169:669–87.

[76] Bose S, Rai DC. Behavior of AAC infilled RC frame under lateral loading. In: 10th US National Conference on Earthquake Engineering, Anchorage, United States of America; 2014.

[77] Leuchars JM, Scrivener JC. Masonry infill panels subjected to cyclic in-plane loading. Bull N Z Natl Soc Earthq Eng 1976; 9(2):122-131.

[78] Schwarz S, Hanaor A, Yankelevsky DZ. Experimental response of reinforced concrete frames With AAC masonry infill walls to in-plane cyclic loading. Structures 2015; 3:306–19.

[79] Zhai C, Kong J, Wang X, Chen ZQ. Experimental and finite element analytical investigation of seismic behavior of full-scale masonry infilled RC frames. J Earthq Eng 2016; 20:1171–98.

[80] Stylianidis KC. Experimental investigation of masonry infilled RC frames. Open Constr Build Technol J 2012; 6(1):194–12.

[81] Cavaleri L, Trapani FD. Cyclic response of masonry infilled RC frames: Experimental results and simplified modeling. Soil Dyn Earthq Eng 2014; 65:224–42.

[82] Baran M, Sevil T. Analytical and experimental studies on infilled RC frames. Int J Phys Sci 2010; 5(13):1981–1998.

[83] Crisafulli F. Seismic behaviour of reinforced concrete structures with masonry infills. Ph.D. Thesis. University of Canterbury, New Zealand; 1997.

[84] Calvi GM, Bolognini D. Seismic response of reinforced concrete frames infilled with weakly reinforced masonry panels. J Earthq Eng 2001; 5:153–85.

[85] Essa ASAT, Badr MRK, El-Zanaty AH. Effect of infill wall on the ductility and behavior of high strength reinforced concrete frames. HBRC J 2014; 10:258–64.

[86] Haider S. In-plane cyclic response of reinforced concrete frames with unreinforced masonry infills. M.Tech Thesis. Rice University, Texas; 1995.

[87] Sigmund V, Penava D. Experimental study of masonry infilled R/C frames with opening. In: 15th World Conference on Earthquake Engineering, Lisbon, Portugal; 2012.

[88] Yuksel E, Teymur P. Earthquake performance improvement of low rise RC buildings using high strength clay brick walls. Bull Earthq Eng 2011; 9(4):1157–1181.

[89] Billington SL, Kyriakides MA, Blackard B, Willam K, Stavridis A, Shing PB. Evaluation of a sprayable, ductile cement-based composite for the seismic retrofit of unreinforced masonry infills. In: ATC & SEI Conference on Improving the Seismic Performance of Existing Buildings and other Structures; 2009.

[90] Mazzoni S, McKenna F, Scott MH, Fenves GL, Jeremic B. OpenSEES command language manual. University of California, Berkeley: Pacific Earthquake Engineering Research Center; 2003.

[91] Mander JB, Priestley MJN, Park R. Theoretical stress-strain model for confined concrete. J Struct Eng 1988; 114(8):1804-1826.

[92] Lehman DE. Performance-based seismic design of well-confined concrete columns. Ph.D. Thesis. University of California, Berkeley; 1998.

[93] Elwood KJ. Modelling failures in existing reinforced concrete columns. Can J Civ Eng 2004; 31:846–59.

[94] Sezen H, Moehle JP. Shear strength model for lightly reinforced concrete columns. J Struct Eng 2004; 130(11):1692–1703.

[95] Sheikh MA. Seismic analysis of masonry infilled RC frame structures with masonry infills. Ph.D. Thesis. Indian Institute of Technology Gandhinagar, India; forthcoming.

[96] Suzuki T, Choi H, Sanada Y, Nakano Y, Matsukawa K, Paul D. Experimental evaluation of the in-plane behaviour of masonry wall infilled RC frames. Bull Earthq Eng 2017; 15:4245–67.

[97] Koutas L, Bousias SN, Triantafillou TC. Seismic strengthening of masonry-infilled RC frames with TRM: Experimental study. J Compos Constr 2015; 19.

[98] Dukuze A, Dawe JL. In-plane stiffness of three-storey three-bay RC Frames with masonry infills. In: 11th International Brick/Block Masonry Conference, Shanghai, China; 1997.

[99] De Risi MT, Di Domenico M, Ricci P, Verderame GM, Manfredi G. Experimental investigation on the influence of the aspect ratio on the in-plane/out-of-plane interaction for masonry infills in RC frames. Eng Struct 2019;189:523–40

[100] Furtado A, Rodrigues H, Arêde A, Varum H. Out-of-plane behavior of masonry infilled RC frames based on the experimental tests available: A systematic review. Constr Build Mater 2018;168:831–48.

[101] Anić F, Penava D, Guljaš I, Sarhosis V, Abrahamczyk L. Out-of-plane cyclic response of masonry infilled RC frames: An experimental study. Eng Struct 2021;238.

[102] André F, Hugo R, Arede A, Varum H. Simplified macro-model for infill masonry walls considering the out-of-plane behaviour. Earthq Eng Struct Dyn 2016:507–24.

[103] Hashemi A, Mosalam KM. Shake-table experiment on reinforced concrete structure containing masonry infill wall. Earthq Eng Struct Dyn 2006:1827-1852.

[104] Hashemi A, Mosalam KM. Seismic Evaluation of Reinforced Concrete Buildings Including Effects of Masonry Infill Walls. PEER Report 2007/100, Pacific Earthquake Engineering Research Center, College of Engineering, University of California, Berkeley; 2007.

[105] Kadysiewski S, Mosalam KM. Modeling of Unreinforced Masonry Infill Walls Considering In-Plane and Out-of-Plane Interaction. PEER Report 2008/102, Pacific Earthquake Engineering Research Center, College of Engineering, University of California, Berkeley; 2009.